RIGHT-ANGLED LINKS IN THICKENED SURFACES

A Dissertation
Submitted to
the Temple University Graduate Board

---

in Partial Fulfillment
of the Requirements for the Degree of
DOCTOR OF PHILOSOPHY

---

by
Rose Kaplan-Kelly
May, 2023

Examining Committee Members:

David Futer, Advisory Chair, Mathematics
Matthew Stover, Mathematics
Samuel Taylor, Mathematics
Anastasiia Tsvietkova, Math and Computer Science, Rutgers University-Newark

ABSTRACT

An overarching goal for studying hyperbolic links is to relate the geometric properties of a link's complement to the combinatorics of its diagrams. Links which admit an alternating diagram, *alternating links*, are especially useful for this study. Alternating links have traditionally been considered with projection diagrams on the 2-sphere and with complements in the 3-sphere but there is a strong (and growing) field of work on generalizations of hyperbolic alternating links to broader classes of projection surfaces and complements in more general 3-manifolds. This thesis research lies within that setting, with a focus on the right-angled structure, totally geodesic surfaces, commensurability, and arithmeticity of a family of links in thickened surfaces.

We consider the geometry of a class of hyperbolic link complements in thickened surfaces built from Euclidean and hyperbolic tilings. Such a link has *right-angled structure* if its complement admits a decomposition into generalized polyhedra with all right-angles that glue to form the complete hyperbolic structure on the complement. Champanerkar, Kofman, and Purcell conjecture that there are no right-angled knots in S^3. We show that this conjecture does not extend to the setting of thickened surfaces by constructing an example.

A surface S in hyperbolic 3-manifold M is *totally geodesic* if any geodesic tangent to S in M is contained in S. Classifying the presence of totally geodesic surfaces in hyperbolic 3-manifolds is a current open problem. Generalizing Gan's

work in the 3-sphere, we define a link to be *right-angled generalized completely realizable (RGCR)* if it has a complement which admits a decomposition into hyperbolic generalized polyhedra with the combinatorics of its checkerboard polyhedra and has right-angled structure. We employ the combinatorics of gluings of generalized hyperbolic bipyramids to prove an equivalence for generalized alternating links in thickened surfaces being RGCR, their complements containing two totally geodesic checkerboard surfaces, their checkerboard surfaces each containing one type of polygon, and the links having diagrams which satisfy a set of restrictions. We then use these diagram restrictions to find bounds on the number of RGCR links or tilings corresponding to RGCR links, in terms of g for each genus g projection surface. Two manifolds, M and M', are *commensurable* if they share a finite-sheeted cover. We show that RGCR links corresponding to equivalent tilings are commensurable and consider the arithmeticity of RGCR links.

ACKNOWLEDGEMENTS

First, I would like to thank my thesis advisor, Dave Futer. Your guidance and enthusiasm have been integral to my journey through the program and to developing my research and professional goals in math. Thank you for your encouragement and for believing in me and my work. I would also like to thank my dissertation committee. In particular, my thanks to Matthew Stover for Proposition 5.8.

Next, I would like to thank my Bryn Mawr geometry and topology professors Lisa Traynor and Paul Melvin, REU mentor Colin Adams, and high school math teacher Barbara Wood. Lisa, Paul, and Colin thank you for your mentorship and for fostering my interest in math research. Barbara, thank you for your fun topics courses and for assigning the project that introduced me to knot theory.

To my fellow graduate students in the Math Department at Temple, especially in the geometry group, thank you for your friendship. I deeply appreciate the community we built.

Finally, I would like to thank my family and my wonderful partner for your love and support.

To Alicia. For making it through the distance and (I'm sure seemingly endless) hours of hyperbolic knot theory.

TABLE OF CONTENTS

LIST OF TABLES

LIST OF FIGURES

CHAPTER 1

Introduction

Throughout this work we will consider *knots*, *links*, and their *complements*.

Definition 1.1. A *knot* is a smooth embedding of S^1 into a 3-manifold Y. A *link* is a smooth embedding of a disjoint union of copies of S^1 into a 3-manifold Y.

Definition 1.2. The *complement* of a knot or link L in 3-manifold Y is $Y \backslash L$, i.e. the space that remains if the link is removed. If we instead remove a neighborhood of the link, $N(L)$, the result is the *link exterior*, $Y \backslash N(L)$.

We traditionally study knots and links by looking at their diagrams on either $\mathbb{R}^2$ or S^2, and their complements in $\mathbb{R}^3$ or S^3. Thurston showed that knots in S^3 fall into one of three types: torus knots, satellite knots, and hyperbolic knots [50]. A *torus knot* is a knot that can be embedded without crossings on an unknotted torus in S^3, a *satellite knot* is a knot that can be embedded non-trivially in a regular neighborhood of another nontrivial knot, and a *hyperbolic knot (or link)* is a knot whose complement admits a complete hyperbolic structure of finite volume. More precisely, if link L is hyperbolic then its complement is isometric to $\mathbb{H}^3/\Gamma$ where Γ is a torsion-free *Kleinian group*, i.e. discrete subgroup of the orientation preserving isometry group of $\mathbb{H}^3$, $PSL_2(\mathbb{C})$ of finite covolume.

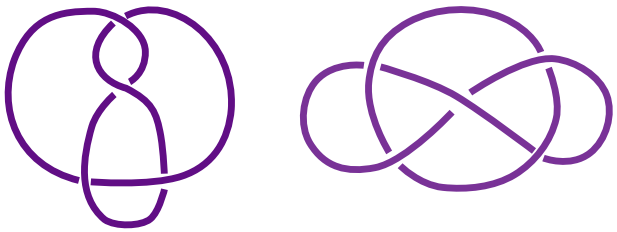

Figure 1.1: Left: An alternating knot. Right: An alternating link.

We will focus on hyperbolic knots and links, which comprise the vast majority of prime knots enumerated up to 19 crossings [10] [25]. In particular, this research falls under the canopy of the overarching question in hyperbolic knot theory of relating the geometric properties of a link's complement to the combinatorics of its diagrams. *Alternating links*, links which admit diagrams in which crossings alternate between over and under as in Figure 1.1, are especially useful for this question. Menasco showed that all prime alternating links are hyperbolic except for $(2, q)-$ torus links [35]. A *checkerboard surface* of an alternating link is a surface formed by connecting faces of the link diagram along twisted bands at the link's crossings as shown (for a generalized alternating link) in Figure 1.2. Menasco and Thurston showed that we can decompose the complements of alternating links along these surfaces [37] [49]. A useful and interesting generalization of alternating links are links with projections which are alternating on higher genus projection surfaces in compact manifolds other than the 3-sphere. This thesis centers on one such family, *cellular weakly generalized alternating links*. We provide the definition of this family of links and survey results on topological and geometric decompositions of their complements due to [26], [27], [11], and [4] in Chapter 2.

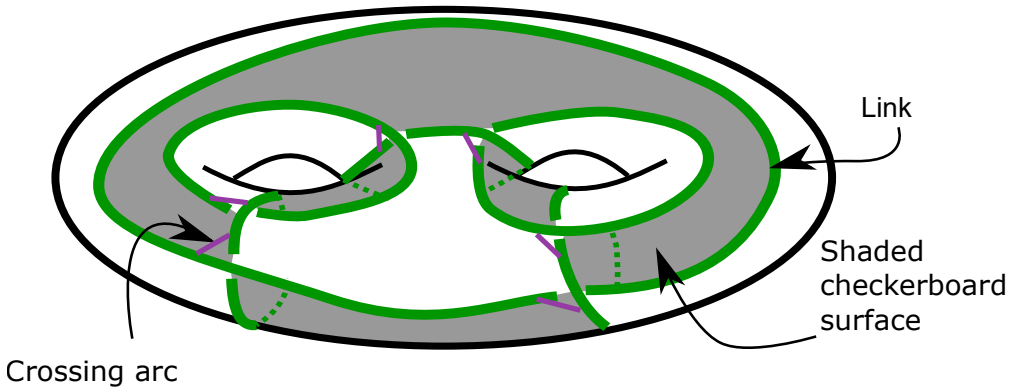

Figure 1.2: A link diagram (in green) on a genus 2 surface. We can form two checkerboard surfaces from this link diagram by connecting faces of the same color via twisted bands at every crossing. These two surfaces (one shaded and one white) meet in *crossing arcs*, running between the under and over-strands of the link.

Aitchison and Reeves introduced the term *completely realizable* to refer to hyperbolic alternating links with complements that admit a *geometric decomposition* by cutting along their checkerboard surfaces [7]. In other words, links that not only decompose into topological pieces along their checkerboard surfaces but into pieces that admit a hyperbolic structure with geodesic boundary modeled on the combinatorics of the original link diagram and re-glue to form the complete hyperbolic structure on the complement. A rich source of completely realizable links are generalized alternating links with regular polygons in their diagrams [4] [11]. In this thesis we study a family of these links and ways to leverage the close relationship between their diagrams and decompositions of their complements to gain geometric information about their complements.

A surface Σ in a link complement M is *totally geodesic* if any geodesic tangent to Σ at any point in M is contained in Σ. The problem of finding, and counting, totally geodesic surfaces in hyperbolic 3-manifolds is a current area of research (see, for example, [36], [8], [5], [31], [30], and [20]). In Chapter 3, we consider the implications of a generalized alternating link complement in a thickened surface containing two totally geodesic checkerboard surfaces, generalizing Gan's work in S^3 [20]. In Theorem 3.7 in Chapter 3, we prove an equivalence for links in thickened surfaces satisfying certain diagram restrictions, their complements containing two totally geodesic surfaces built from the link diagram, and their complements having right-angled structure. We call links satisfying these properties *right-angled generalized completely realizable (RGCR)* links.

Champanerkar, Kofman, and Purcell associated a set of hyperbolic right-angled polyhedra to any prime alternating link diagram in S^3 and proved that we can use these right-angled polyhedra to determine a lower bound on the volume of the complements of these links [12]. They conjecture that there does not exist a right-angled knot in S^3 [12, Conjecture 5.12]. Providing evidence for this conjecture, Gan proved that there are no right-angled completely realizable knots in S^3 [20, Theorem 3.14]. In Theorem 3.9 in Chapter 3, we show that an RGCR knot does exists in the setting of thickened surfaces.

Gan showed that there are precisely three right-angled completely realizable links in S^3 [20]. Champanerkar, Kofman, and Purcell found that there are precisely

two classes of links in the thickened torus with a diagrammatic restriction that have this right-angled structure [11]. In Chapter 4, we find an upper bound on the number of RGCR links for each projection surface with negative Euler characteristic. We also include a table listing the tilings and fundamental domains corresponding to these right-angled links with projection surfaces of genus $2-7$ in Chapter 6.

Two hyperbolic manifolds are *commensurable* if they admit a common finite-sheeted cover. Arithmeticity is defined and discussed in Chapter 5. There has been significant work on determining the commensurability and arithmeticity of different families of link complements (see, for example, [53], [21], [38], [46]). Reid and Walsh conjecture that the set of knots commensurable to a hyperbolic knot in S^3 has at most 3 elements [53]. In Chapter 5, we investigate the commensurability and arithmeticity of RGCR links. In Proposition 5.3, we show that RGCR links with the same types of polygons in their checkerboard surfaces are commensurable. We then provide examples of geometric triangulations of some classes of RGCR links and use one of these triangulations to find a family of arithmetic RGCR links in Theorem 5.9.

CHAPTER 2

Generalized Alternating Links and their Decompositions

This chapter surveys work on weakly generalized alternating links from [4], [11], [26], and [27]. In the first section, we give the definition of this family of links, following [26] and [27]. In the second section, we outline a topological decomposition of their complements from [27]. For the final section, we describe results about the geometric structure on their complements from [4], [11], and [27].

2.1 Weakly Generalized Alternating Links

We are interested in generalizing the class of alternating links in S^3 to links with projections which are alternating on higher genus surfaces in broader classes of 3-manifolds. Several authors have studied different such generalizations. Adams considered toroidally alternating links, a generalization of alternating links to projections on a Heegaard torus [6]. Hayashi [24] and Ozawa [41] independently studied links with projections on higher genus surfaces. Howie introduced (in S^3), and then Howie and Purcell extended, the definition of *weakly generalized alternating links*, which we will focus on in this work. Howie showed that in S^3 weakly generalized

alternating links are nontrivial, nonsplit, and prime [26]. Howie and Purcell found decompositions for weakly generalized alternating link complements, gave conditions that determine when they are hyperbolic, and thereby showed that weakly generalized alternating links in thickened surfaces with diagrams in which complementary regions are disks are hyperbolic [27, Theorem 4.2]. We discuss the hyperbolicity of these complements in more detail in Section 2.3.

Kalfagianni and Purcell considered the volumes of these links. Alternating links in S^3 have volumes that are bounded above and below in terms of their twist number [29]. Kalfagianni and Purcell showed that this holds for weakly generalized alternating links in thickened surfaces as well. However, they also found a family of weakly generalized alternating links with projection surface a Heegaard surface of genus 2 and complement in S^3 that do not have such an upper bound on their volumes [28].

Throughout this thesis we will assume that our projection surface, F, is a connected, closed, orientable, surface with non-positive Euler characteristic. We will assume our links to be in the thickened surface $F \times I$ with generalized projection diagram $\pi(L)$ on $F \times \{0\}$ and specify the genus g of the surface as needed. We will use the following definitions adapted from [27] for this setting.

Definition 2.1. The generalized diagram $\pi(L)$ of a link L on surface F with genus $g \geq 1$ is *weakly prime* if for any disk D in F with ∂D that intersects the link diagram transversely exactly twice, $\pi(L) \cap D$ is an embedded arc.

Definition 2.2. The diagram $\pi(L)$ is *cellular* if all complementary regions, called faces, on F are disks.

Definition 2.3. A generalized diagram is *alternating* if the boundary of each region of $F\backslash\pi(L)$ can be given an orientation such that crossings alternate between under and over.

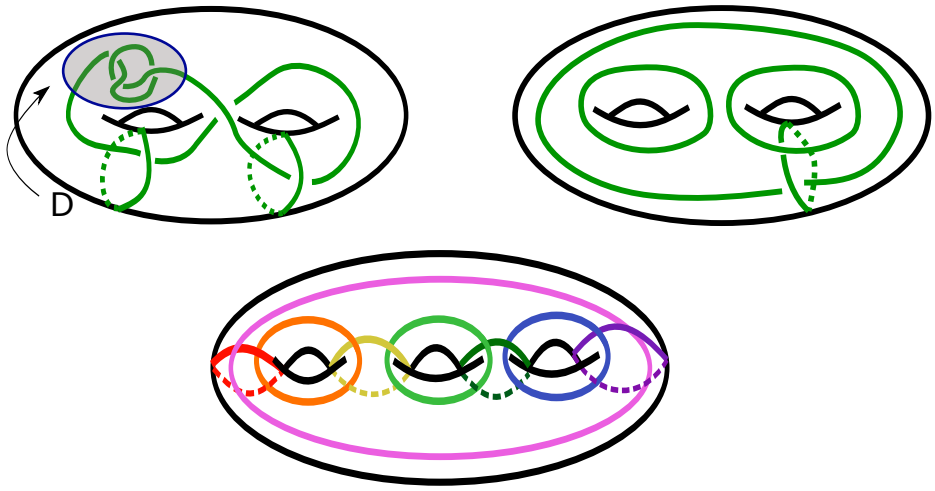

Figure 2.1: Above: Links (in green) which do not satisfy the weakly prime (left) and cellular (right) conditions. Below: A cellular weakly generalized alternating link.

Orient each region of $F\backslash\pi(L)$ such that the induced orientation on the boundary runs from under-crossings to over-crossings. Next, color the faces white or shaded depending on whether their orientation is clockwise or counter-clockwise. The result of this coloring will be that faces which share an edge have opposite orientations, and therefore are different colors, while faces that are diagonal from each other with respect to a crossing have the same color. This coloring is called a

checkerboard coloring of the generalized link diagram. A link with a generalized diagram on F that is weakly prime, cellular, and alternating is also checkerboard colorable.

Definition 2.4. Given a generalized diagram $\pi(L)$ with a checkerboard coloring, we can form two *checkerboard surfaces*. Insert a twisted band at each crossing of $(F \times I) \backslash L$ to connect all shaded faces. The result is a surface composed of shaded faces with boundary the link. Perform the same procedure for the white faces. The result is two surfaces that intersect in arcs in $(F \times I) \backslash L$ at each crossing. These *crossing arcs* run between the under-strand and over-strand of L as shown in Figure 1.2.

Definition 2.5. A generalized diagram $\pi(L)$ is *reduced alternating* if it is alternating, weakly prime, and every component of L projects to at least one crossing of $\pi(L)$.

Note that if our link diagram is alternating, weakly prime, and cellular then it is reduced alternating as well but reduced alternating diagrams need not be cellular. Howie and Purcell call links that are reduced alternating and checkerboard colorable *weakly generalized alternating*, with the additional criteria that the links satisfy a so-called representativity condition [27]. This condition will always hold for our setting in thickened surfaces because F has no compression disks in $F \times I$.

2.2 Topological Decompositions

Our main tool for studying the complements of cellular weakly generalized alternating links will be to exploit properties of their topological and geometric decompositions and the relationship they have to the links' diagrams. In this section we will describe the generalized polyhedral decompositions of cellular weakly generalized alternating link complements given in [27], [11], and [4]. These decompositions generalize Thurston and Menasco's work on polyhedral decompositions of alternating link complements in S^3 (see [49, Chapter 3] and [37]) and Adams' work on bipyramid decompositions of link complements in S^3 [3]. We begin with some definitions.

Definition 2.6. A *polyhedron* P is a closed 3-ball with a finite graph G on its boundary. The graph G contains a finite number of vertices and edges and the regions of $\partial P \backslash G$ are simply connected *faces*. An *ideal polyhedron* is a polyhedron with all vertices removed.

In order to generalize polyhedral decompositions of link complements in S^3 to link complements in thickened surfaces, we need the notion of *generalized polyhedra*.

Definition 2.7. A *generalized polyhedron* is homeomorphic to $(F \times [0,1])/(F \times \{1\})$ with a cellular graph Γ on $F \times \{0\}$. An *ideal generalized polyhedron* is a generalized polyhedron with the vertices of Γ and the vertex at

$F \times \{1\}$ removed. A *semi-truncated generalized polyhedron* is a generalized polyhedron with the vertices of Γ and a neighborhood of the vertex at $F \times \{1\}$ removed. When F has genus 1, we will have ideal generalized polyhedra, also called *ideal torihedra* in [11]. When F has genus greater than 1, we will have semi-truncated generalized polyhedra.

We will decompose our link complements into topological generalized polyhedra. For projections on a torus, Champanerkar, Kofman, and Purcell constructed a decomposition of the link complement into two ideal torihedra and a decomposition into ideal tetrahedra [11]. Adams, Calderon, and Mayer found a bipyramid decomposition of generalized alternating links in thickened surfaces of genus $g \geq 0$ [4]. Considering even broader classes of generalized alternating link complements, Howie and Purcell found a chunk decomposition [27]. For ease of reading we will usually refer to 'generalized polyhedra' to indicate any of the types of generalized polyhedra and further specify when the vertex types become pertinent.

First, we define a map that will be useful throughout this work. Note that this map matches that of alternating links on S^2 in S^3 (see [49]).

Definition 2.8. A gluing by *gear shift rotation* is a map between two generalized polyhedra, P^+ and P^-, such that each pair of corresponding n-gon faces on P^+ and P^- are identified with a $1/n$ rotation either clockwise or counterclockwise.

Next, we state a restriction of Howie and Purcell's Propositions 3.1 and 3.3 in [27] to our setting of thickened surfaces and give their proof.

Proposition 2.9. *(Howie-Purcell [27, Propositions 3.1 and 3.3]). Let F have genus $g > 0$ and L be a cellular weakly generalized alternating link in $F \times I$ with projection diagram $\pi(L)$. Then $(F \times I)\backslash L$ decomposes into two ideal torihedra or two semi-truncated generalized polyhedra, P^+ and P^-, satisfying:*

- *P^+ and P^- are homeomorphic to $F \times [0, 1)$ and $F \times (-1, 0]$ with a finite set of points removed from each $F \times \{0\}$ boundary.*
- *On each copy of F there is an embedded graph in which vertices, edges, and regions correspond to $\pi(L)$. The vertices are ideal and 4-valent.*
- *The faces $F\backslash\pi(L)$ on P^+ and P^- admit a coloring correspond to the checkerboard coloring of $\pi(L)$.*
- *$(F \times I)\backslash L$ is the result of gluing P^+ to P^- by a homeomorphism between the copies of $F\backslash\pi(L)$ on their boundaries. This homeomorphism is the composition of the identity with a rotation on each face of $F\backslash\pi(L)$. One can choose an orientation such that white faces are rotated to their neighboring edge clockwise, while shaded faces are rotated to their neighboring edge counterclockwise.*
- *Edges correspond to crossing arcs and are glued in collections of four. Each ideal vertex has pairs of opposite edges which are glued together.*

Proof. Take four copies of the crossing arc at each crossing of $\pi(L)$ and orient each to run from the understrand to the overstrand of L. Next isotope the crossing

arcs to lie in F and identify pairs of crossing arcs which are on the same side of the overstrand at each crossing. Note that this identification depends on whether our perspective is from 'above' or 'below' as this changes which strand of L is considered the overstrand at a crossing (see Figure 2.2).

Next, slice the complement along F. This decomposes the complement into two generalized polyhedra P^+ and P^- which are homeomorphic to $(F \times I) \backslash N(F)$. Now shrink each overstrand of L to a vertex corresponding to its crossing. Each overstrand is now an ideal vertex and the crossing arcs are stretched to now match the original graph of $\pi(L)$. The faces of P^+ and P^- correspond to the diagram graph with the edges of the graph formed by crossing arcs.

We can rebuild the full complement from this decomposition by gluing P^+ to P^- with a rotation on each face, namely following the gear shift map (see Figure 2.3). □

2.3 Geometric Decompositions

We are interested in not only the topological structure of link complements in thickened surfaces but also in their geometry. Adams et al. proved that links in thickened surfaces satisfying generalized prime and alternating conditions are hyperbolic [1]. Howie and Purcell showed that a broader class of generalized alternating link com-

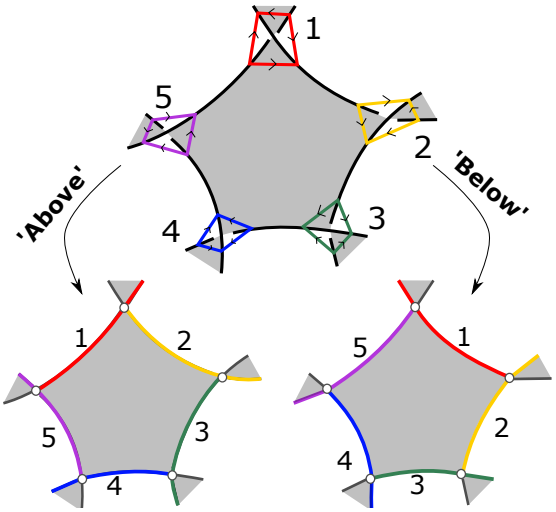

Figure 2.2: Above: 4 copies of a crossing arc for each crossing on a pentagonal face of a link diagram. Below: The view of the pentagonal face from 'above' and 'below' after the overstrands of the link are shrunk down to ideal vertices.

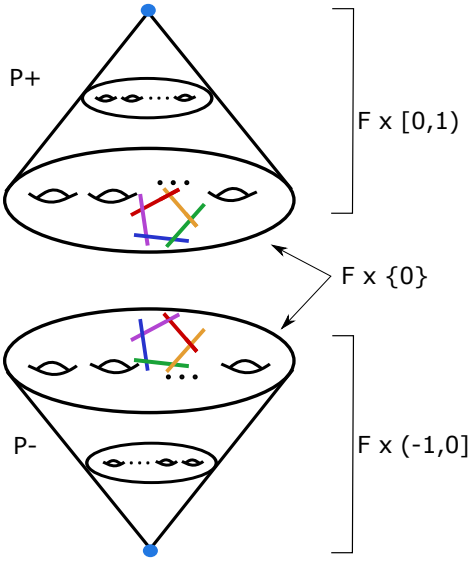

Figure 2.3: Generalized polyhedra P^+ and P^-. A face on each of their surface boundaries is drawn with edges colored to show their gluing identifications. If F is a torus then the apexes are ideal. If F has negative Euler characteristic then we truncate the ultra-ideal apexes of P^+ and P^- to get the surface boundary components $F \times \{1\}$ and $F \times \{-1\}$.

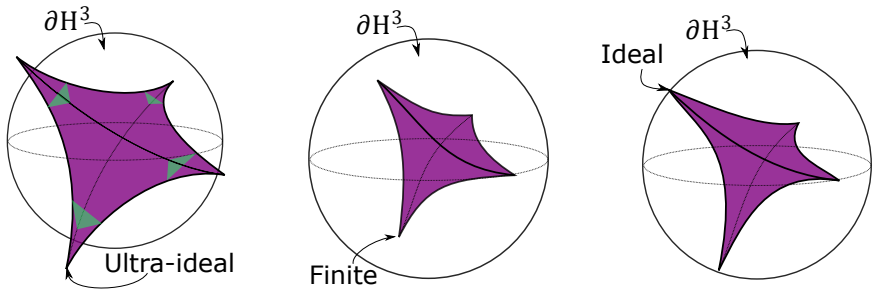

Figure 2.4: Hyperbolic tetrahedra with all ultra-ideal, ideal, or finite vertices.

plements are hyperbolic in [27, Theorem 4.2]. We state a restriction of their theorem below:

Theorem 2.10. *(Howie–Purcell, [27, Theorem 4.2]). Let $\pi(L)$ be a cellular weakly generalized alternating projection of a link, L, on a closed surface, F, of genus at least one in $Y := F \times [-1, 1]$. Then $Y \backslash L$ is hyperbolic.*

In this section we describe a family of cellular weakly generalized alternating links corresponding to regular Euclidean and hyperbolic tilings and outline the work in [4] (also independently shown in [11] for $F = T^2$) on directly finding geometric decompositions of their complements. We will consider the complete hyperbolic structure on the link complements with totally geodesic boundary.

Definition 2.11. We say that a generalized polyhedron is *hyperbolic* if it admits a convex hyperbolic structure with totally geodesic faces. A hyperbolic generalized polyhedron can have finite, ideal, or ultra-ideal vertices, when the vertices lie within $\mathbb{H}^3$, on the boundary of $\mathbb{H}^3$, or outside of $\partial\mathbb{H}^3$, respectively (see Figure 2.4). In the case when the generalized polyhedra have ultra-ideal vertices, we can truncate the

ultra-ideal vertices to form totally geodesic boundary faces. These totally geodesic boundary faces are the intersection of the generalized polyhedra with the unique truncation planes perpendicular to the edges meeting at each ultra-ideal vertex.

Definition 2.12. A *geometric decomposition* of $(F \times I)\backslash L$ is a topological decomposition such that each generalized polyhedron has a hyperbolic structure and the set of generalized hyperbolic polyhedra re-glue to form the complete hyperbolic structure on $(F \times I)\backslash L$ with totally geodesic boundary.

That the complements have one complete hyperbolic structure with totally geodesic boundary follows from Mostow–Prasad Rigidity:

Theorem 2.13. *(Mostow–Prasad Rigidity, see [39] and [43]). Let M and N be complete finite volume hyperbolic n-manifolds for $n \geq 3$. Then any isomorphism between their fundamental groups, $\pi_1(M)$ and $\pi_1(N)$, is realized by a unique isometry.*

Theorem 2.14. *(Folklore, [4, Theorem 2.5]). Let M be a finite volume anannular hyperbolic 3-manifold with boundary. Then there exists a complete hyperbolic structure with totally geodesic boundary on M and it is unique up to isometry.*

Proof. Assume M is a finite volume anannular (i.e. not containing any essential annuli) hyperbolic 3-manifold with boundary. Double M along its boundary and call the result DM. Then DM is a finite volume hyperbolic 3-manifold by geometrization [50]. By Mostow–Prasad rigidity, this complete hyperbolic structure on DM is

unique. DM admits an orientation-reversing homeomorphism by reflecting in ∂M. By [52, Theorem 7.1] this homeomorphism is isotopic to an isometry. Thus, also following from Mostow–Prasad Rigidity, ∂M is totally geodesic. □

Now that we know that the complements of cellular weakly generalized alternating links in thickened surfaces have a unique complete hyperbolic structure with totally geodesic boundary, the question that naturally follows is how to explicitly find it. We can accomplish this for links with regular faces in their diagrams by examining how the generalized polyhedra in their decompositions are glued (see [49, Section 3.10] and [45, Chapter 4]) and considering the *cusps* of the complements.

Definition 2.15. A *cusp* of $M := (F \times I)\backslash L$ is a neighborhood of ∂M homeomorphic to $T^2 \times [0, 1)$. A *cusp torus* is the boundary of cusp.

Theorem 2.16. *(see [49, Section 3.10]). Let $M := (F \times I)\backslash L$. The hyperbolic structure on M is complete if and only if for each cusp of M, the induced structure on the toroidal boundary of the cusp is a Euclidean structure on the torus.*

We define a regular polygon as in [7].

Definition 2.17. Let T be a convex, planar, ideal, polygon with n sides. Then T is *regular* if it is set-wise invariant under a rotation of order n.

Definition 2.18. A *regular ideal n-bipyramid* is an ideal polyhedron formed by coning a regular ideal polygon to upper and lower ideal apexes (see Figure 2.5). A generalized regular n-bipyramid may have ideal or ultra-ideal apexes. We will refer

to the polygon the bipyramid is built on as its *horizontal face*, and the faces sharing the ideal or ultra-ideal apexes as its *vertical faces*.

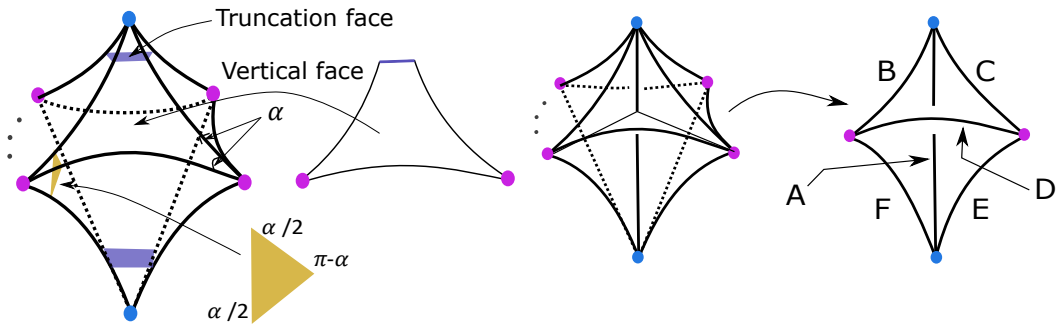

Figure 2.5: Left: A generalized bipyramid with interior angle α in its horizontal face. Truncation faces for a neighborhood of the apexes of this bipyramid are shown in dark blue. Half of a truncation face for one of the ideal vertices corresponding to the strands of the link is shown in yellow. Right: A wedge of a generalized bipyramid with edges labeled.

Links corresponding to regular tilings of $\mathbb{E}^2$ and $\mathbb{H}^2$ are especially well suited for finding a hyperbolic generalized bipyramid decomposition.

Definition 2.19. A *tiling* of $\mathbb{X} = \mathbb{E}^2$ or $\mathbb{H}^2$ is a partition of the space into polygonal *tiles* or *faces*. The tiles have disjoint interiors. If they intersect on their boundaries, they either share an edge and two vertices or they share one vertex. Two tilings, T and T', are equivalent if there exists a homeomorphism $h : \mathbb{X} \to \mathbb{X}$ which sends the vertices, edges, and faces of T to T'.

For this work we will restrict our attention to 4-*valent tilings*, meaning that precisely four tiles meet at every vertex of the tiling. Following [14] we will denote the *vertex type* of a vertex v by $[a, b, c, d]$ for a, b, c, d the numbers of sides of the

four polygons meeting at v in clockwise order. If our tiling has only one vertex type then we will refer to this tiling as an $[a, b, c, d]$ *tiling*.

Definition 2.20. We say that link L *corresponds to a tiling* T of $\mathbb{X} = \mathbb{E}^2$ or $\mathbb{H}^2$ if there is a torsion free subgroup of the symmetry group of T, Γ, such that $\mathbb{X}/\Gamma$ is a surface tiled by the polygons in T and L is the result of resolving the vertices of this tiling into crossings in an alternating manner. Such a choice of crossings exists and is well-defined when our link has a checkerboard coloring because we can choose for strands of L to run from undercrossings to overcrossings in the clockwise or counterclockwise orientation for the white and shaded faces, respectively.

Remark 2.21. Adams, Calderon, and Mayer call links corresponding to a regular tiling of $S^2, \mathbb{E}^2$, or $\mathbb{H}^2$ with a k transitivity classes of vertices *alternating k-uniform tiling links*. Champanerkar, Kofman, and Purcell call links corresponding to biperiodic edge-to-edge Euclidean tilings with convex regular polygons *semi-regular links* [11]. These links have also been referred to as *textile links* [9].

We state Adams, Calderon, and Mayer's theorem below and outline their proof.

Theorem 2.22. *(Adams–Calderon–Mayer, Lemma 2.10 and Theorem 4.4). Let L be a link in $F \times I$ corresponding to a tiling T by regular polygons of S^2, $\mathbb{E}^2$, or $\mathbb{H}^2$. Let $\{F_i\}$ be the collection of m non-bigon faces complementary to the projection of L to F and let n_i be the number of edges in the i-th face. Then:*

1. *Topologically,* $(F \times I) \backslash L$ *decomposes into* m *face-centered bipyramids, each corresponding to a unique face with* n_i *edges.*

2. *The complete hyperbolic structure on* $(F \times I) \backslash L$ *(with totally geodesic boundary when* F *has negative Euler characteristic) is obtained by gluing together symmetric hyperbolic bipyramids, each corresponding to a face of the tiling of* F*.*

Proof. Begin by taking the topological decomposition of the link complement into two generalized polyhedra, P^+ and P^- as in Proposition 2.9.

Next, cone each face on the boundary of these generalized polyhedra (corresponding to the link diagram $\pi(L)$) to subdivide P^+ and P^- into two collections of pyramids with the same ideal apex if $F = T^2$ and ultra-ideal apex if F has higher genus. The links of the ideal or ultra-ideal vertices are polygons with interior angles determined by the interior angles of each face the pyramids are built upon. We can see this by noting that if F has a hyperbolic structure, then the truncation plane is the unique hyperbolic plane perpendicular to the collection of edges of the pyramid with an endpoint at that apex. If F is a torus, then $F \times \{1\}$ and $F \times \{-1\}$ get their Euclidean structures from the truncated faces of bipyramids with ideal apexes. For a fixed interior angle there is only one regular hyperbolic polygon up to isometry and one regular Euclidean polygon up to similarity. Both $F \times \{-1\}$ and $F \times \{1\}$ are the result of gluing these regular boundary polygons. So, the boundary surfaces have the same geometric structure as the projection surface.

Glue the collection of pyramids in pairs along their faces corresponding to $\pi(L)$. The result is a collection of generalized bipyramids decomposing the complement. Next, we will show that these bipyramids glue together along isometric faces, the dihedral angles around each edge have a sum of 2π, and the links of the equatorial vertices of the bipyramids fit together to induce a Euclidean structure on each of the cusps of $(F \times I)\backslash L$.

If $F = T^2$ then all vertical faces are ideal triangles and thus isometric (see [49, Section 3.9]). If F has negative Euler characteristic then the vertical faces are hyperbolic quadrilaterals with angles $0, 0, \pi/2, \pi/2$. One edge of this quadrilateral (shared with the horizontal face of the bipyramid) is a crossing arc, two edges have one ideal vertex (corresponding to the link) and one finite vertex (corresponding to the truncation face of the bipyramid) and one edge is finite (shared with the truncation face). See Figure 2.5. This finite edge of the vertical face determines the face up to isometry and thus vertical faces corresponding to regular horizontal faces are isometric. Now glue wedges along their vertical faces on the same side of each overstrand at each crossing (see Figure 2.6). Under this face identification, all vertical and horizontal edges are identified in collections of 4. (Note that the finite edges of the truncation faces are identified in pairs.) The dihedral angle at each vertical edge is the α_i interior angle of the horizontal face it is built upon (see Figure 2.5). Therefore the sum of the dihedral angles on the vertical edges which are identified is the sum of the interior angles of the set of 4 horizontal faces

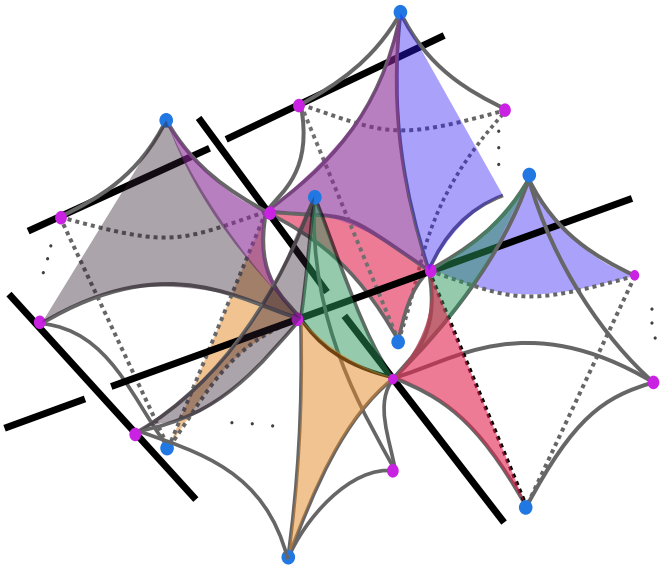

Figure 2.6: Four generalized bipyramids centered on the faces surrounding a crossing of link L (shown in black). The vertices in blue are either ultra-ideal or ideal while the ideal vertices corresponding to the strands of L are pink. The face identifications for the (generalized) bipyramids are indicated by their coloring (see also Figure 11 in [4]).

surrounding a crossing. These faces correspond to a hyperbolic or Euclidean tiling and thus must have interior angles which sum to 2π about every crossing. The dihedral angles for the horizontal (crossing arc) edges are all $\pi - \alpha_i$, as shown in Figure 2.5, because every truncation face for the ideal vertices is Euclidean. Therefore the sum of the dihedral angles on the vertical edges is also 2π.

Next, consider the truncation quadrilaterals for every ideal vertex corresponding to the strands of the link (i.e. the vertices of the horizontal face of each bipyramid). Each of these quadrilaterals has interior angles α_i and $\pi - \alpha_i$. Using the symmetry of the bipyramids we see that these faces have equal side lengths and are thus a collection of rhombi. Under the identification of the faces of the bipyramids, these

rhombi are glued into a Euclidean tiling in which vertices corresponding to vertical edges are glued and vertices corresponding to horizontal edges are glued. The angles of the rhombi about these vertices sum to $4\pi - (\sum \alpha_i) = 2\pi$ about the vertices corresponding to horizontal edges and $\sum \alpha_i = 2\pi$ for the vertices corresponding to vertical edges. This implies that the hyperbolic structure on $(F \times I) \backslash L$ obtained from gluing together the hyperbolic structures on these face-centered bipyramids is a complete hyperbolic structure (possibly with totally geodesic boundary). □

Figure 2.7 gives an example of this geometric decomposition.

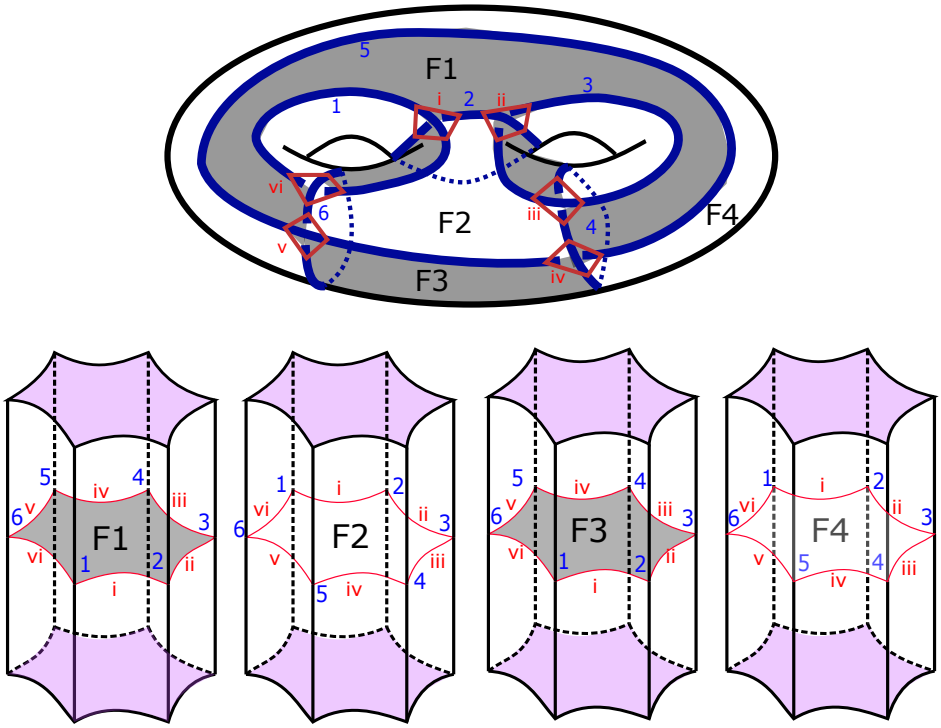

Figure 2.7: A geometric truncated bipyramid decomposition of a link in $F \times I$ with $g = 2$. The strands of the link (labeled in dark blue) correspond to the ideal vertices of the horizontal faces of each truncated bipyramid (with their shading from the checkerboard coloring). The truncation faces of each bipyramid, which glue to form the boundary surfaces $F \times \{1\}$ and $F \times \{-1\}$, are shown in lavender.

CHAPTER 3

Totally Geodesic Surfaces and Right-Angled Structure

In this chapter we consider links with totally geodesic checkerboard surfaces and links whose complements admit a complete hyperbolic structure formed by gluing generalized checkerboard polyhedra with $\pi/2$ dihedral angles. We show an equivalence for a link having a complement with this right-angled structure, its checkerboard surfaces being totally geodesic, and it admitting a diagram satisfying a set of restrictions. We then find an example of a right-angled knot in a thickened surface.

3.1 Totally Geodesic Checkerboard Surfaces

Definition 3.1. Let Σ be a properly embedded essential surface in hyperbolic 3-manifold M and let $\rho : \pi_1(M) \to PSL_2(\mathbb{C})$ be a discrete, faithful representation. Then Σ is *totally geodesic* if the image of $\pi_1(\Sigma)$ under the induced representation is Fuchsian (i.e. conjugate to a discrete subgroup of $PSL_2(\mathbb{R})$).

The existence and number of embedded or immersed totally geodesic surfaces in hyperbolic 3-manifolds is an interesting question with useful applications. For instance, by [8, Theorem 1.1], if a finite volume hyperbolic 3-manifold M con-

tains infinitely many totally geodesic surfaces then it is arithmetic. Menasco and Reid found that the complement in S^3 of a prime, connected, alternating link cannot contain a closed embedded totally geodesic surface. Moreover, they conjecture that the complement of a hyperbolic knot in S^3 does not admit a closed, embedded, totally geodesic surface [36]. Gan showed that if alternating links in S^3 have two totally geodesic checkerboard surfaces then they meet at right-angles [20, Theorem 3.3]. In this section we generalize Gan's work to consider cellular weakly generalized alternating links with two totally geodesic checkerboard surfaces and the implications this has for the geometric structure on their complements.

Definition 3.2. A link L is *completely realizable* if the complete hyperbolic structure on $(F \times I)\backslash L$ is given by gluing hyperbolic generalized polyhedra by gear shift rotation and these hyperbolic generalized polyhedra have the combinatorial structure of the generalized checkerboard polyhedra of $\pi(L)$.

Lemma 3.3. *Let L be a cellular weakly generalized alternating link. If $\pi(L)$ has two totally geodesic checkerboard surfaces then L is completely realizable and the hyperbolic generalized checkerboard polyhedra associated to $\pi(L)$ are isometric.*

Proof. We claim that there is a hyperbolic generalized polyhedron with the combinatorial structure of the generalized checkerboard polyhedra associated to $\pi(L)$. First, consider the generalized checkerboard polyhedron P^+. Lift P^+ to $\mathbb{H}^3$ and consider a fundamental domain, $\widehat{P^+}$. There is a fixed angle between the link diagram's totally geodesic checkerboard surfaces and thus between the faces of this

generalized polyhedron. Since both checkerboard surfaces are totally geodesic, we find that any region S, consisting of an n-gon and its interior in one of the checkerboard surfaces, lifts to an ideal n-gon $\widehat{S}$ in $\widehat{P^+}$. The ideal vertices of this lift are distinct, which implies that none of the boundary faces of P^+ collapse in the preimage.

The other generalized checkerboard polyhedron associated to $\pi(L)$, P^-, has the same dihedral angles between its totally geodesic faces as P^+. Additionally, the boundary components of both generalized polyhedra are incompressible because both copies of F have no compression disks in $F \times I$. We can therefore apply [47, Theorem 8.15] to see that P^+ and P^- must have the same complete hyperbolic structure with totally geodesic surface boundary. This implies that there is a hyperbolic generalized polyhedron with the combinatorial structure of P^- and this realization of P^-, $\widehat{P^-}$, is the mirror image of $\widehat{P^+}$. Both hyperbolic generalized polyhedra have the combinatorial structure of the topological checkerboard polyhedra and therefore glue by gear shift rotation on their totally geodesic faces to give the complete hyperbolic structure on the link complement. □

Observe that if both hyperbolic generalized polyhedra are right-angled then there is a quick way in which to show that they are isometric [47, Lemma 8.14]. Take P^+ and double it along first its shaded checkerboard surface and then along its white checkerboard surface. The result is a finite volume hyperbolic manifold, $D_w D_s(P^+)$, with totally geodesic boundary and cusps corresponding to the com-

ponents of L. By Mostow–Prasad rigidity $D_w D_s(P^+)$ has a unique hyperbolic structure. Using that both checkerboard surfaces are totally geodesic, we see that reflecting in either checkerboard surface in $D_w D_s(P^+)$ is an isometry. Therefore we can construct an isometry between P^+ and P^- by reflecting on both checkerboard surfaces.

Theorem 3.4. *Let L be a cellular weakly generalized alternating link with generalized checkerboard polyhedra P^+ and P^-. If L has two totally geodesic checkerboard surfaces then the faces of P^+ and P^- are regular.*

Proof. By Lemma 3.3, L is completely realizable. Therefore the complete hyperbolic structure on $(F \times I)\backslash L$ is given by gluing two generalized checkerboard polyhedra, P^+ and P^-, by gear shift rotation. Call the totally geodesic faces of P^+, T_i, and the faces of P^-, T_i'.

We follow Gan's proof [20, Theorem 3.14]. The gear shift rotation provides us with a collection of gluing isometries $\{\psi_i : T_i \to T_i'\}$. These isometries, which are rotations, glue the faces without shearing on any edge because L is completely realizable.

By Lemma 3.3, the generalized checkerboard polyhedra P^+ and P^- are isometric. Consider the restriction of the isometry, $\phi : P^- \to P^+$, to the copy of $F\backslash\pi(L)$ on the boundary of P^-. We find our isometry by reflecting across the totally geodesic checkerboard surfaces whose boundaries are the link diagram, so ϕ

will fix $\pi(L)$. This implies that the two copies of $F\backslash\pi(L)$ have the same geometric structure induced by the hyperbolic structure on P^+ and P^-.

Now consider the collection of maps $\phi \circ \psi_i : T_i \to T_i$. First, ψ_i rotates and glues T_i to T_i', then ϕ sends T_i' back to T_i. The result is an isometry of each totally geodesic face T_i which is an order n rotation. □

The following is a slight generalization of Gan's Lemma [20, Lemma 3.9]. We follow the proof from [20] adjusted for this setting.

Proposition 3.5. *Let L be a cellular weakly generalized alternating link with diagram $\pi(L)$. Suppose that the two checkerboard surfaces of $\pi(L)$ are totally geodesic in $(F \times I)\backslash L$. If G_n, G_m are an n-gon and m-gon in the diagram that are diagonal from each other, then $n = m$. In other words, polygons in the same totally geodesic checkerboard surface have the same number of sides.*

Proof. By Theorem 3.4 the polygons in the checkerboard surfaces are regular. By assumption G_n and G_m are diagonal from each other with respect to a vertex in $\pi(L)$ so they are part of the same totally geodesic checkerboard surface. Suppose that this is the white checkerboard surface Σ_W. Lift both faces to $\mathbb{H}^3$. The result will be totally geodesic polygons which are adjacent up to translations by the lifts of Σ_W. Consider the pre-image such that the faces share an edge with vertices at 0 and ∞, as shown in Figure 3.1.

Choose the cusp sizes such that all of their boundaries have a meridian of the same length in the Euclidean metric induced from the complete hyperbolic structure

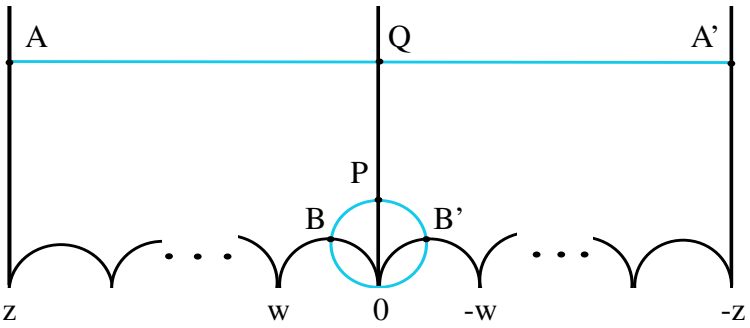

Figure 3.1: Figure modified from [20]. Lifts of G_n and G_m in $\widehat{\Sigma_W}$ are shown as a vertical plane in the upper half-space model. The intersection of $\widehat{\Sigma_W}$ with the boundaries of horoball lifts of a neighborhood of L appear in blue and the polygons appear in black.

on the link complement. The link diagram's two totally geodesic checkerboard surfaces give the boundary of each cusp a tiling by quadrilaterals with interior angle the angle between the two totally geodesic checkerboard surfaces of $\pi(L)$. One such tiling is shown in Figure 3.2. Using that this angle is fixed and that the totally geodesic surfaces are embedded, we see that the quadrilaterals have parallel sides. Consider one cusp. One of the diagonals of all of the parallelograms on this cusp's boundary corresponds to a meridian on the boundary of a tubular neighborhood of the link component corresponding to this cusp. Therefore one diagonal of each parallelogram is the same length. So, adjacent parallelograms have sides of the same (respective) lengths. This is shown in Figures 3.2 and 3.3.

In Figure 3.1 we see that the sides AQ and QA' are the same length, as are BP and PB'. We have the following consecutive vertices of $\widehat{G_n}$: $z, \infty, 0, w$ where z and w are complex. Using that the segments are of equal length, we see that $-z, \infty, 0,$ and $-w$ are the corresponding symmetric consecutive vertices of $\widehat{G_m}$.

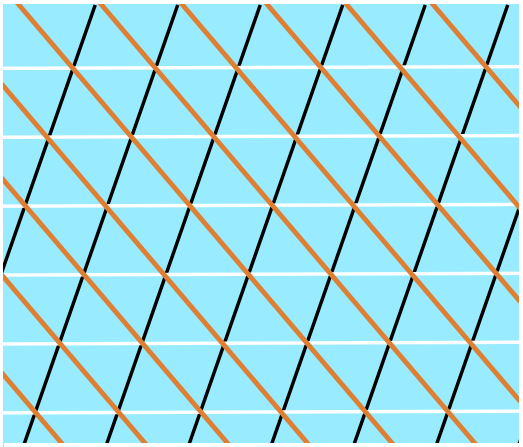

Figure 3.2: A tiling of the boundary of a cusp by its intersection with the white and shaded totally geodesic checkerboard surfaces. The cusp is shown in blue, the intersection with lifts of the white checkerboard surface are shown in white, and the intersection with lifts of the shaded checkerboard surface are shown in black. The pre-image of the meridian, the diagonal of each parallelogram that is the same fixed length, is shown in orange.

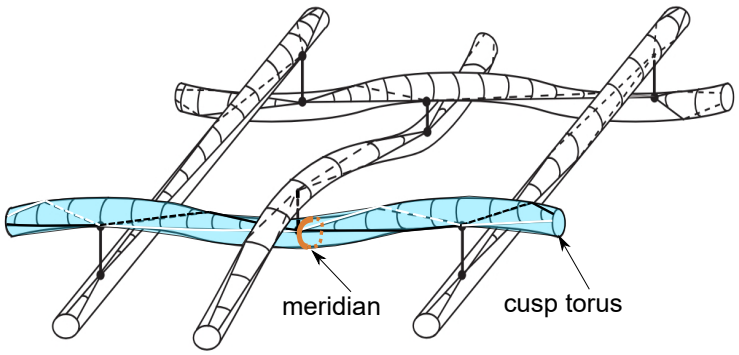

Figure 3.3: Figure modified from [2] and [20]. Tiling of the boundary of cusps of $(F \times I)\backslash L$ by quadrilaterals. A meridian is shown in orange.

So, $\widehat{G_n}$ and $\widehat{G_m}$ have consecutive vertices with the same cross ratio. Aitchison and Reeves showed that a hyperbolic polygon with x sides is regular if and only if the cross ratio of any four consecutive vertices of the polygon is $1+1/(2\cos(2\pi/x)+1)$ [7, Lemma 3.2]. Our two sets of vertices have the same cross ratio so our two lifted polygons then have the same number of sides. □

3.2 Right-Angled Structure

3.2.1 RGCR Links

We begin with a few more definitions generalizing the definition of a completely realizable link given in [7] and of Gan's right-angled completely realizable links [20, Definition 3.13].

Definition 3.6. If, in addition to being completely realizable, all dihedral angles in both generalized checkerboard polyhedra of $\pi(L)$ are right-angles, then we say that the link is *right-angled generalized completely realizable* (RGCR).

Theorem 3.7. *Let L be a cellular weakly generalized alternating link on F in $F \times I$. Then the following are equivalent:*

1. *L is RGCR.*
2. *L has two totally geodesic checkerboard surfaces.*
3. *The checkerboard surfaces of $\pi(L)$ each have exactly one type of polygon.*

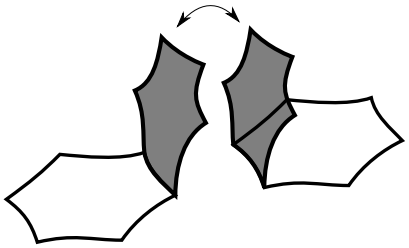

Figure 3.4: Identifying faces with the same color on generalized polyhedra P^+ and P^- forces the faces of the other color to meet at a π angle.

4. *L has a projection diagram $\pi(L)$ on F with at most two types of polygons, one with n sides and the other with m sides, such that the polygons are arranged in an $[n, m, n, m]$ pattern about each vertex and are regular.*

Proof. $(1) \implies (2)$ By assumption the complete hyperbolic structure on the link complement is given by gluing P^+ and P^- by gear shift rotation. Consider the totally geodesic faces of these hyperbolic generalized polyhedra. If we glue just the shaded faces of P^+ and P^- then we see that the white faces meet in pairs at a π angle which is the sum of the two $\pi/2$ dihedral angles between white and shaded faces on each hyperbolic generalized polyhedron (see Figure 3.4). This also holds if we glue only the white faces. Therefore the checkerboard surfaces of $\pi(L)$ are both totally geodesic and the hyperbolic structure on each checkerboard surface is determined by the hyperbolic structure of the generalized polyhedra.

$(2) \implies (3)$ Follows from Proposition 3.5.

$(3) \implies (4)$ The checkerboard surfaces of $\pi(L)$ each contain one type of polygon, therefore $\pi(L)$ must have faces consisting of polygons of n numbers of

sides and m numbers of sides in a pattern $[n, m, n, m]$ about each vertex. If the faces are regular then we are done.

Suppose that the polygons are not regular. If F has negative Euler characteristic then the link diagram on F in $F \times I$ corresponds to a quotient of a tiling of $\mathbb{H}^2$ by n-gons and m-gons arranged in the specified pattern. Call this tiling T. This $[n, m, n, m]$ pattern about each vertex of the tiling satisfies condition (1) in [14]. Therefore there exists a tiling of $\mathbb{H}^2$, T', by regular polygons with vertex type $[n, m, n, m]$ at every vertex, which is equivalent to T [14, Lemma 2.5]. Using this regular tiling of $\mathbb{H}^2$ we find the diagram of L with regular polygons on F. If $F = T^2$ we apply the same argument using [15, Theorem 1.3] to find $\pi(L)$ as the quotient of a regular tiling of $\mathbb{E}^2$.

$(4) \implies (1)$ By assumption, we can construct L as a quotient of a regular tiling of $\mathbb{E}^2$ or $\mathbb{H}^2$ with one vertex type. Decompose the complement into generalized bipyramids. Adams, Calderon, and Mayer found the angles of these bipyramids in terms of the angles of the polygons in $F \backslash \pi(L)$ by cutting each bipyramid into a collection of wedges with angles $D = \pi - \alpha$, $B = C = E = F = \alpha/2$, and $A = 2\pi/n$ for each n-gon in the projection diagram with interior angle α (see Figure 2.5 for labels).

We have assumed that there are two n-gons and two m-gons about each vertex. This implies that for α_n the interior angle of the n-gon and α_m the interior angle of the m-gon, $2\alpha_n + 2\alpha_m = 2\pi$ so $\alpha_n + \alpha_m = \pi$. Slice the generalized bipyramids

along the (horizontal) checkerboard surface faces. We can then see that P^+ and P^- will be the result of gluing the resulting pyramids on their (vertical) faces. This gluing matches the corresponding D edges with dihedral angles $(\pi - \alpha_n)/2$ and $(\pi - \alpha_m)/2$. Using that $(\pi - \alpha_n + \pi - \alpha_m)/2 = \pi/2$, we see that this gluing forms right-angled generalized checkerboard polyhedra. Hence L is right-angled generalized completely realizable. □

Corollary 3.8. *For projection surface $F = T^2$, L is RGCR if and only if it is the triaxial link or the square weave.*

Proof. Theorems 3.7 and 3.4 imply that any RGCR link with alternating projection on the torus is semi-regular. We can then apply [11, Theorem 5.1]. □

3.2.2 Right-Angled Knots

Hyperbolic 3–manifolds with complements that admit a right-angled structure have useful properties. For instance, as we have seen, if M admits a right-angled decomposition, then it must contain an immersed totally geodesic surface from gluing the faces of its (generalized) polyhedra [12]. The family of fully augmented links have a right-angled decomposition that has been used to gain information about their cusps (see [44]) and hidden symmetries (see [38]).

It is a challenging problem to determine in general that a class of hyperbolic 3-manifolds is not right-angled. Gan showed that among alternating links in S^3 there are no right-angled completely realizable knots [20, Theorem 3.14]. Champanerkar,

Kofman, and Purcell conjecture that there does not exist a right-angled knot in S^3 [12, Conjecture 5.12]. However, this will not extend to links in thickened surfaces.

Theorem 3.9. *There exists a right-angled knot in a thickened surface.*

Proof. We construct a right-angled knot in a thickened genus 2 surface in Figure 3.5. This knot corresponds to a hyperbolic tiling by regular octagons. □

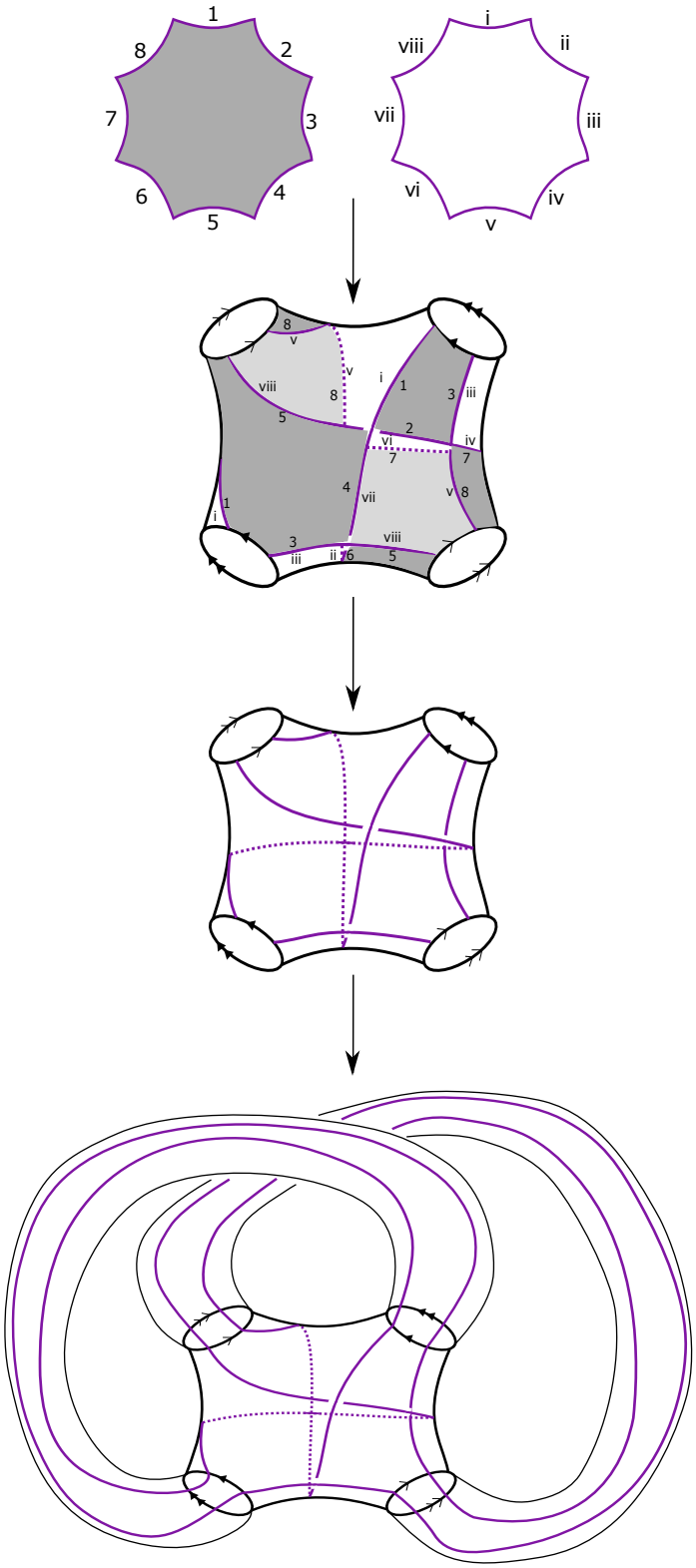

Figure 3.5: An RGCR knot.

CHAPTER 4

Counting RGCR Links

Gan showed that there are only three right-angled completely realizable links alternating on S^2 in S^3 [20]. See Figure 4.1. In the thickened torus, we saw in Corollary 3.8 that there are only two tilings that correspond to RGCR links. A question that naturally follows is if there are similarly few RGCR links and tilings corresponding to RGCR links for thickened surfaces with genus greater than one. Here, we answer that question by finding an upper bound.

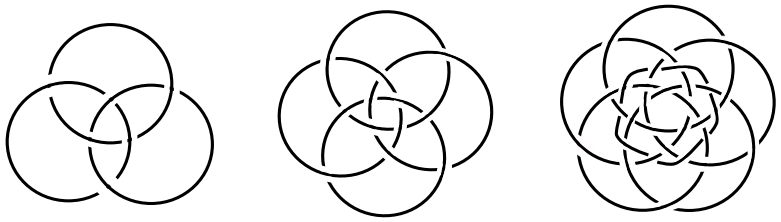

Figure 4.1: The three right-angled completely realizable links in S^3. (Also see Figure 6 in [20].)

Definition 4.1. Denote the number of times that n-gons occur in a checkerboard surface of a link diagram by k_n and the number of times that m-gons occur in the other checkerboard surface by k_m.

We will use the restrictions from Theorem 3.7 on the types of polygons that appear in each link diagram for our bound. In an RGCR link diagram each n-gon

shares all of its edges with an m-gon and similarly each m-gon corresponds to m n-gons. So, $k_n n = k_m m$. When $n = m$, we have $k_n = k_m$. We next use the area of the polygons and the Euler characteristic of the projection surface F.

Proposition 4.2 (Gauss–Bonnet)**.** *Let F be the projection surface of a link L with polygons T_n and T_m in its diagram. Then $-2\pi\chi(F) = a(F) = k_n a(T_n) + k_m a(T_m)$, where a denotes area.*

Theorem 4.3. *Given a projection surface F of genus g, there are finitely many tilings of $\mathbb{H}^2$ and $\mathbb{E}^2$ which correspond to RGCR links, L, with $\pi(L)$ on F. Moreover, for each F of genus $g > 1$, the number of RGCR links is bounded above by* $\left(\frac{310g^2}{9} - \frac{101g}{3} + 4\right)[(84g - 83)!]$.

Proof. By Corollary 3.8 and [11, Theorem 5.1] when F is a torus the only Euclidean tilings which correspond to RGCR links are $[3, 6, 3, 6]$ and $[4, 4, 4, 4]$.

Consider when $g > 1$. First, we will bound the number of fundamental domains of tilings that correspond to RGCR links for a given F with fixed genus g. In other words, we will bound the number of tuples (m, n, k_m, k_n) which correspond to RGCR links in terms of g.

Without loss of generality, assume that $n \leq m$. Then we have that $n \geq 3$ and $m \geq 5$ because the $[n, m, n, m]$ tiling is hyperbolic and the links do not have bigons.

Recall that $\alpha_n + \alpha_n = \pi$ and that $nk_n = mk_m$. Using Gauss–Bonnet we find,

$$\begin{aligned} -2\pi(2-2g) = -2\pi\chi(F) &= a(F) \\ &= \sum^{k_n} a(T_n) + \sum^{k_m} a(T_m) \\ &= k_n(n(\pi-\alpha_n)-2\pi) + k_m(m(\pi-\alpha_m)-2\pi) \\ &= k_n(n(\pi-\alpha_n)-2\pi) + \left(\frac{k_n n}{m}(m\alpha_n - 2\pi)\right). \end{aligned}$$

Simplifying we find

$$4(g-1) = k_n\left(n-2-\frac{2n}{m}\right), \tag{4.1}$$

and

$$4(g-1) = k_m\left(m-2-\frac{2m}{n}\right). \tag{4.2}$$

Equations (4.1) and (4.2) imply that k_n and k_m are determined by n, m, and g. Therefore it suffices for us to find an upper bound on the number of pairs (m,n). In order to do so, we will first find upper bounds on n and on m in terms of g.

Our assumption that $n \leq m$ implies that there is only one option for n and m with $k_n = 1$. Namely, if $k_n = 1$, then $n = m = 4g$ by (4.1) because our assumption that $n \leq m$ implies that $k_n \geq k_m$.

When $k_n \geq 2$,

$$n - 2 - \frac{2n}{m} = \frac{4(g-1)}{k_n} \leq \frac{4(g-1)}{2} = 2g-2,$$

simplifying, we find that

$$n\left(\frac{m-2}{m}\right) \leq 2(g-1)+2 = 2g.$$

Recall that $m \geq 5$, so $\frac{3}{5} \leq \frac{m-2}{m}$. Therefore,

$$n\left(\frac{3}{5}\right) \leq n\left(\frac{m-2}{m}\right) \leq 2g,$$

which implies that $n \leq \frac{10g}{3}$.

We bound m by starting with Equation (4.2). The same set of inequalities hold except with n replaced with m, $n \geq 3$, and $k_m \geq 1$. Therefore,

$$m\left(\frac{1}{3}\right) \leq m\left(\frac{n-2}{n}\right) \leq \frac{4(g-1)}{1} + 2 = 4g-2.$$

Thus, $m \leq 12g-6$.

Our goal is to bound the number of possible pairs (m,n) for each fixed genus g. Using that $n \geq 3$ and that there is only the one option for (m,n) with a value of n larger than $10g/3$ (the case when $n = m$ and $k_n = 1 = k_m$), there are up to $\frac{10g}{3} - 2 + 1 = \frac{10g-3}{3}$ choices for n. Using that $m \geq 5$, there are $12g-6-4 = 12g-10$ choices for m.

For each $m \leq \frac{10g}{3}$ there are $m-2$ choices for what n can be and for each $m \geq (10g)/3$ there are $\frac{10g-3}{3}$ possibilities for n. Therefore the number of pairs (m,n) is bounded above by:

$$\left[\sum_{m=5}^{(10g)/3}(m-2)\right] + ((10g-3)/3)(12g-6-((10g)/3))$$
$$= \left[\sum_{m=5}^{(10g)/3}(m-2)\right] + (\frac{2}{9}(10g-3)(13g-9))$$
$$= \frac{310g^2}{9} - \frac{101g}{3} + 4.$$

We show in Figure 4.2 that distinct links can have the same tuple (m,n,k_m,k_n). So, we also need to bound the number of RGCR links that correspond to the same tiling T. The orientation preserving symmetry group of T is finitely generated by two rotations preserving the checkerboard coloring. This group of symmetries is the orientation preserving subgroup of the triangle group which is all of the symmetries of T. The RGCR links corresponding to this tiling are then the result of taking the quotient of $\mathbb{H}^2$ by surface subgroups of this symmetry group of the same index. By the $84(g-1)$ Theorem this index x satisfies, $x \leq 84(g-1)$ (see [18]). The number of subgroups of index x of a finitely generated group G is bounded above by $x \cdot x!^{d(G)-1}$, where $d(G)$ is the minimal number of generators of G [32]. Therefore the number of weakly generalized alternating links on F that correspond to T is bounded by $x \cdot x!^{d(G)-1} = x \cdot x! \leq (x+1)! \leq (84g-83)!$. □

An alternative method that we could use to find a bound on the number of RGCR links corresponding to a given tiling (with a specified number of polygons in their

checkerboard surfaces) is to consider the number of feasible identifications of the faces in the checkerboard surfaces along their edges. However, this method quickly results in a larger upper bound as k_n and k_m increase. The sets of fundamental domains of tilings corresponding to RGCR links with projection surfaces of genus $2-7$ are listed in Table 6.1.

Remark 4.4. We cannot bound k_n and k_m for an RGCR link on the torus with these calculations. Using the Euler characteristic we see that $\chi(F) = 0 = v - e + f = \frac{2e}{4} - e + f = \frac{2mk_m}{4} - mk_m + (k_n + k_m)$, where v, e, and f, are the number of vertices, edges, and faces in the 4-valent graph corresponding to the link diagram on F. Simplifying, we find that $2k_n + (2-m)k_m = 0$. So the only restriction we get from m (or similarly from n) is that $k_n = k_m$ when $n = 4 = m$ and $k_n = 2k_m$ when $m = 6$ and $n = 3$.

Example 4.5. Figure 4.2 provides an example of two distinct links on a genus 3 surface which derive from the same tiling of $\mathbb{H}^2$ by octagons and contain the same number of octagons in their projection diagrams. We can check that the links are distinct by noting that they have different numbers of components.

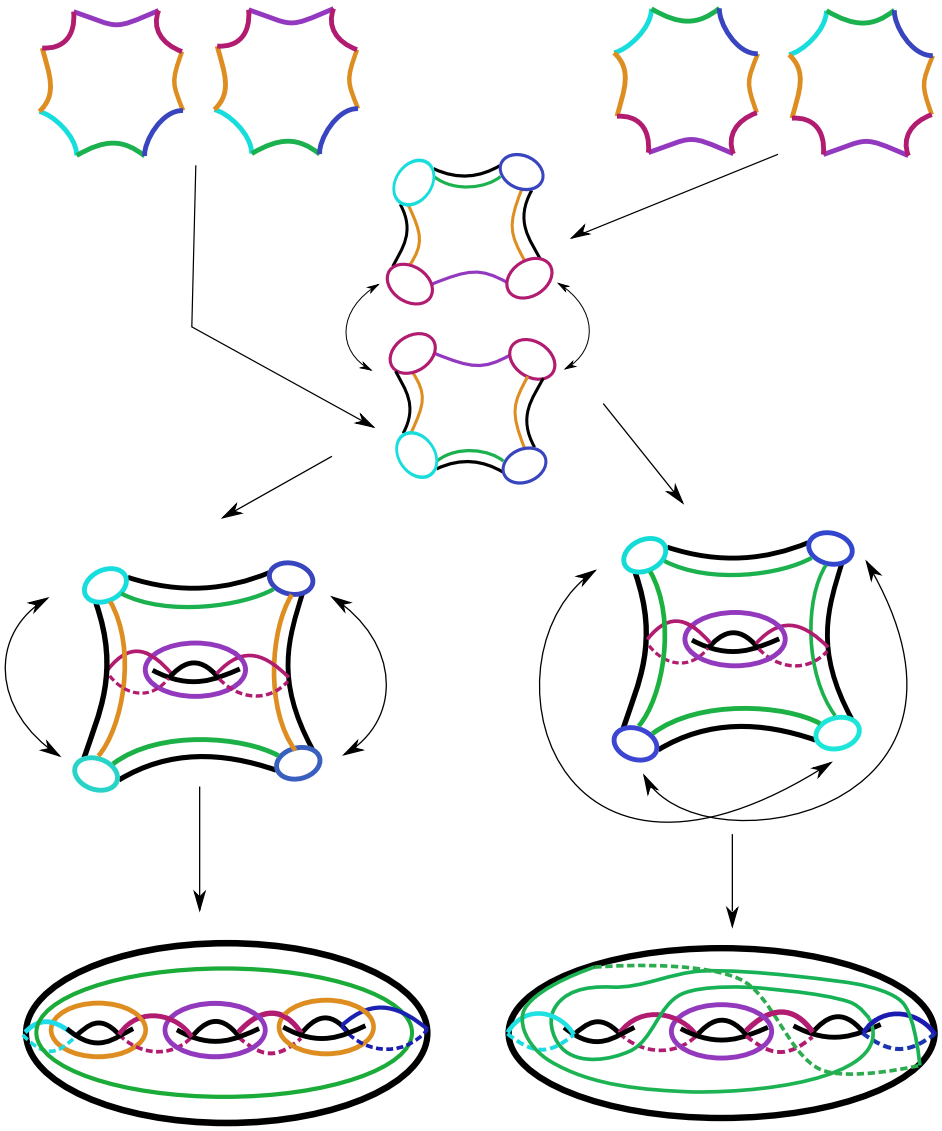

Figure 4.2: Two links from a tiling of $\mathbb{H}^2$ by right-angled octagons. Both links have $m = 8 = n$ and $k_n = 2 = k_m$. We begin with a fundamental domain of four right-angled octagons and proceed to identify edges to form the projection diagrams of the links. Double headed arrows indicate gluing while single headed arrows indicate the results of the gluings. Different choices of gluing form distinct links.

CHAPTER 5

Arithmeticity, Commensurability, and Triangulations

The commensurability classes and arithmeticity of different families of knot and link complements have been considered by many authors including in [11], [46], [21], [38]. In this chapter we introduce commensurability and arithmeticity following Neumann and Reid's exposition in [40] and Walsh's exposition in [53]. We then consider the commensurability classes and arithmeticity of RGCR links. We determine that RGCR links corresponding to all but two hyperbolic tilings are non-arithmetic, find a family of arithmetic RGCR links, and show that RGCR links corresponding to the same tiling are commensurable.

5.1 Commensurability of RGCR Links

We begin by defining commensurability:

Definition 5.1. Two hyperbolic manifolds (or orbifolds) are *commensurable* if they admit isometric finite-sheeted covers. Restricting to finite volume hyperbolic manifolds $M \cong \mathbb{H}^3/\Gamma$ and $M' \cong \mathbb{H}^3/\Gamma'$ with Γ and Γ' discrete subgroups of Isom$(\mathbb{H}^3)$, it follows that M and M' are commensurable if and only if Γ and a conjugate of Γ' have a common finite index subgroup.

Commensurability is an equivalence relation and therefore provides a way to classify hyperbolic manifolds. Moreover, these classes provide information about different properties of hyperbolic manifolds which are preserved or related under commensurability. For example, for finite volume hyperbolic 3-manifolds, commensurable manifolds have volumes which are rationally related [33].

In order to determine the commensurability classes of RGCR links with projection diagrams of genus greater than 1, we will consider the double of their complements along their totally geodesic surface boundary. Note that the doubled complements then contain at least six embedded totally geodesic surfaces, in particular, two corresponding to the surfaces that previously were part of the boundary (and now are contained within the doubled complement), and four corresponding to the two sets of checkerboard surfaces. First, we address the relationship between the commensurability class of a manifold and that of its double.

Lemma 5.2. *Let M and M' be cellular weakly generalized alternating link complements with doubles DM and DM'. If M and M' are commensurable then DM and DM' are commensurable.*

Proof. If M and M' are commensurable then they share a finite-sheeted cover, Y. Double Y along its totally geodesic surface boundary components and call the result DY. The double DY is a common finite-sheeted cover of DM and DM'. □

Proposition 5.3. *Consider $RGCR$ links with projection surface F of genus greater than 1. All $RGCR$ links with the same n and m-gon faces in their checkerboard surfaces are commensurable.*

Proof. By Theorem 3.7 any two RGCR links, L_1 and L_2, with the same n and m-sided polygons correspond to regular $[n, m, n, m]$ tilings of $\mathbb{H}^2$. The group of isometries of this tiling is the collection of hyperbolic isometries generated by reflecting in the three sides of a triangle with angles π/n, π/m, and $\pi/2$. We can see this by noting that these isometries preserve the $[n, m, n, m]$ tiling and that any isometry of the tiling is the result of a combination of these reflections, as shown for tilings consisting of one type of polygon in [16].

Doubling this triangle along the edge between the π/n and π/m angles gives us a quadrilateral in the graph corresponding to $\pi(L)$ which corresponds to two bipyramid wedges sharing a horizontal edge in the hyperbolic structure of each link's complement (see Figure 5.1). Reflections in the faces of this pair of wedges are then isometries of the three-dimensional tiling of $\mathbb{H}^3$ by the bipyramids corresponding to the $[n, m, n, m]$ tiling. The complement of L_1 in $F_1 \times I$, M_1, and the complement of L_2 in $F_2 \times I$, M_2, both finitely cover the orbifold which is the quotient of the three-dimensional tiling by these these isometries. Take the intersection of $\pi_1(M_1)$ and $\pi_1(M_2)$. The result is a group G corresponding to a finite cover of M_1 and M_2. □

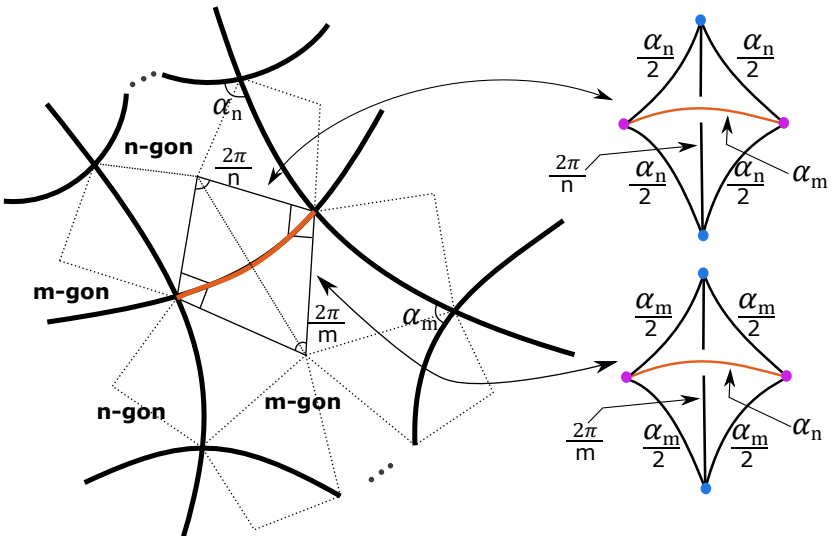

Figure 5.1: Left: Neighboring n-sided and m-sided faces in an $[n, m, n, m]$ tiling. The isometries of the tiling are generated by reflecting in a π/n, π/m, $\pi/2$ triangle. Double this triangle along the edge running between the center of the n-gon and the m-gon. The result is a quadrilateral with interior angles $\frac{2\pi}{n}$, $\frac{2\pi}{m}$, and $\pi/2$. Right: Wedges corresponding to n-gon and m-gon faces of this tiling that share a horizontal (crossing arc) edge shown in orange.

5.2 Arithmeticity and Geometric Triangulations

We next turn to the arithmeticity and ideal triangulations of RGCR links. Throughout this section, $M \cong \mathbb{H}^3/\Gamma$ will be a cusped finite volume hyperbolic manifold.

Definition 5.4. M is *arithmetic* if Γ is an arithmetic Kleinian group, namely, commensurable to $PSL_2(\mathcal{O}_d)$ for $\mathcal{O}_d$ the ring of integers of $\mathbb{Q}(\sqrt{-d})$ where d is positive and square-free.

Another characterization of arithmeticity uses the *commensurator* of Γ, $\mathrm{Comm}(\Gamma) = \{g \in \mathrm{Isom}(\mathbb{H}^3) \mid [\Gamma : \Gamma \cap g\Gamma g^{-1}] < \infty\}$. From Margulis' work, $\mathrm{Comm}(\Gamma)$ is discrete in $\mathrm{Isom}(\mathbb{H}^3)$ if and only if Γ is non-arithmetic [34]. This im-

plies that non-arithmetic finite volume hyperbolic 3-manifolds are commensurable if and only if they cover a common quotient orbifold, namely $\mathcal{O} \cong \mathbb{H}^3/\text{Comm}(\Gamma)$.

In their study of links with alternating projections on the torus, Champanerkar, Kofman, and Purcell classified the arithmeticity and commensurability classes of semi-regular links based on the types of polygons in their corresponding tilings. They prove these results in part by calculating the *invariant trace fields* of the link complements. The *invariant trace field*, $k\Gamma := \mathbb{Q}(tr(\gamma^2)|\gamma \in \Gamma)$, of M is a commensurability invariant which ties together number theoretic and geometric ways of studying hyperbolic link complements [33]. The geometric viewpoint arises from a theorem of Neumann and Reid who showed that we can use a *geometric ideal triangulation* of M to generate the invariant trace field.

Definition 5.5. A *geometric ideal triangulation* of M is a decomposition of the manifold into positively oriented ideal hyperbolic tetrahedra, $\{T_i\}$, glued together by orientation-reversing isometries along their faces.

Every ideal tetrahedron is parametrized by a complex number z_j. We can see this by applying an isometry mapping our ideal tetrahedron to the ideal tetrahedron with vertices 0, 1, ∞, and z_j as shown in Figure 5.2.

Let $k_\Delta\Gamma := \mathbb{Q}(z_j \mid j = 1, ..., n)$ for $\{z_i\}$ the set of tetrahedral parameters of a geometric triangulation of M. Neumann and Reid proved that $k\Gamma = k_\Delta\Gamma$ and therefore we can calculate the invariant trace field by finding the tetrahedral parameters of a geometric triangulation of the manifold [40, Theorem 2.4]. For cusped

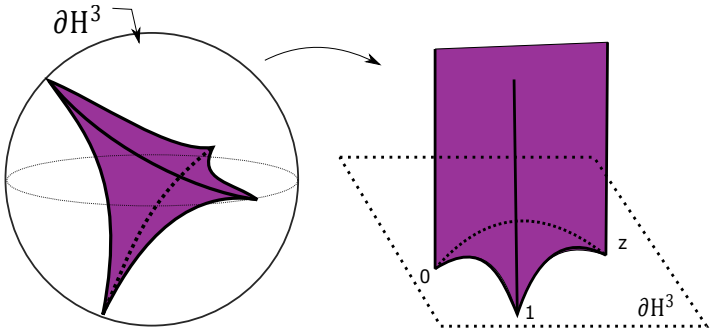

Figure 5.2: An ideal tetrahedron in the ball model of $\mathbb{H}^3$ (left) sent to an ideal tetrahedron with vertices at ∞, 0, 1, and z in the upper half-space model of $\mathbb{H}^3$ (right).

arithmetic hyperbolic 3-manifolds, the invariant trace field is a complete commensurability invariant [33].

We state Champanerkar, Kofman, and Purcell's theorem on the invariant trace fields, arithmeticity, and commensurability of semi-regular links below and outline their proof.

Theorem 5.6. *(Champanerkar–Kofman–Purcell [11, Theorem 4.1]). For a semi-regular link $\mathcal{L}$ with no bigons, with alternating quotient link L, let $M = (T^2 \times I)\backslash L$ and let $k(M)$ denote its invariant trace field.*

1. *If the fundamental domain of the tiling corresponding to $\mathcal{L}$ contains only squares, then $k(M) = \mathbb{Q}(i)$, and M is commensurable to the Whitehead link complement. Hence, M is arithmetic. In this case, $\mathcal{L}$ is the square weave.*

2. *If the fundamental domain of the tiling corresponding to $\mathcal{L}$ contains only triangles and hexagons, then $k(M) = \mathbb{Q}(i\sqrt{3})$, and M is commensurable to*

the figure-8 knot complement. Hence, M is arithmetic. In this case, $\mathcal{L}$ is one of infinitely many semi-regular links.

3. *If the fundamental domain of the tiling corresponding to $\mathcal{L}$ contains at least one hexagon and one square, then $k(M) = \mathbb{Q}(i, \sqrt{3})$. Hence, M is not arithmetic. Assuming v_{tet} and v_{oct} are rationally independent, there are infinitely many commensurability classes of semi-regular links with this invariant trace field.*

Proof. By [11, Lemma 3.3] the Euclidean tilings corresponding to semi-regular links with no bigons have vertex types: $[3, 3, 6, 6], [3, 6, 3, 6], [3, 4, 4, 6], [3, 4, 6, 4]$ and $[4, 4, 4, 4]$.

Begin by decomposing the complement of each type of semi-regular link into ideal hyperbolic bipyramids centered on each face of the link diagram as described in Chapter 2 and given in [11, Theorem 3.5]. The ideal bipyramids further decompose into ideal tetrahedra if we insert an edge running between the apexes of each bipyramid. The shapes of the resulting ideal tetrahedra are $e^{i\pi/2}$ and $e^{i\pi/3}$. We can then apply [40, Theorem 2.4] to find the invariant trace fields of each of the listed types of links.

Next, Snap (see [13]) verifies that one of the complements in the commensurability class of M where L has only square faces (i.e. a quotient of the square weave) is arithmetic. Then M is a cusped finite volume arithmetic manifold with the same invariant trace field as the Whitehead link. The invariant trace field is a complete

commensurability invariant for arithmetic links (see [33, Section 8.4]) so all of the links in this class are arithmetic and commensurable to the Whitehead link.

There are infinitely many distinct Euclidean tilings corresponding to semi-regular links with hexagonal and triangular faces [22]. We can find them by stacking different configurations of parallelograms consisting of half of a regular Euclidean hexagon and a regular Euclidean triangle (see Figure 5.3 or Figure 10 in [11]). These parallelograms are related by reflections and π-rotations and the bipyramids

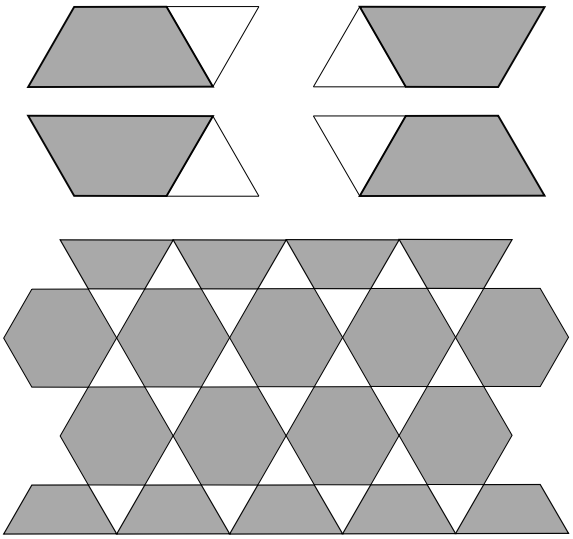

Figure 5.3: Above: Parallelograms which can be stacked to form semi-regular Euclidean tilings with square and hexagonal faces. Below: An example of such a tiling. Also see Figures 9 and 10 in [11] and Figure 4 in [22].

built on each face will be as well. So, the complements of these links are commensurable. Snap verifies that the quotient of the triaxial link is arithmetic. Therefore all links in this commensurability class are arithmetic, finite volume, and have the

same invariant trace field as the figure-8 knot complement. This implies that they are commensurable to it.

Now consider a pair of semi-regular links L_1 and L_2 which both have diagrams that contain at least one square and one hexagon. The complements of these links decompose into ideal regular tetrahedra and ideal regular octahedra. So the volumes of their complements are $(p_1 v_{tet} + q_1 v_{oct})$ and $(p_2 v_{tet} + q_2 v_{oct})$ for p_1, q_1, p_2, and q_2 integers. If v_{tet} and v_{oct} are rationally independent, we can then show that there are infinitely many distinct pairs L_1 and L_2 such that these volumes are not rationally related, and thus the links are not commensurable. □

Remark 5.7. The assumption of rational independence in this theorem stems from Milnor's conjecture that v_{oct} and v_{tet} are rationally independent. This is a special case of the last remaining open question of Thurston's survey article [50].

We next address the arithmeticity of all RGCR links.

Proposition 5.8. *RGCR links corresponding to all* $[n, m, n, m]$ *tilings except for* $[4, 4, 4, 4]$, $[3, 6, 3, 6]$, $[6, 6, 6, 6]$ *and possibly* $[6, 4, 6, 4]$ *are non-arithmetic.*

Proof. First, recall that semi-regular RGCR links correspond to the tiling of $\mathbb{E}^2$ by squares or by hexagons and triangles by Corollary 3.8. These classes of links are arithmetic [11, Theorem 4.1].

Suppose that $M \cong \mathbb{H}^3/\Gamma$ is an arithmetic doubled complement of an RGCR link with projection surface F of genus ≥ 2. Then M has imaginary quadratic invariant

trace field, $\mathbb{Q}(\sqrt{-d})$ [33, Theorem 8.2.3]. Let G be a subgroup of Γ corresponding to one of the closed totally geodesic surfaces in M which was part of the boundary the RGCR link complement was doubled along. Then G is a non-elementary Fuchsian subgroup of the arithmetic Kleinian group Γ, so G is arithmetic [33, Theorem 9.5.2]. The invariant trace field of G is the intersection of the invariant trace field of M, $\mathbb{Q}(\sqrt{-d})$, with $\mathbb{R}$ [33, Corollary 9.5.3]. Therefore G is an arithmetic Fuchsian group with invariant trace field $\mathbb{Q}$. This subgroup G corresponds to the projection surfaces of the original RGCR link complement and thus to a hyperbolic tiling of the form $[n, m, n, m]$ by Theorem 3.7. So, G is commensurable to triangle group $(2, n, m)$. Using Takeuchi's classification of arithmetic triangle groups, we see that this triangle group can only be $(2, 4, 6)$ or $(2, 6, 6)$ [48]. Thus G can only correspond to a hyperbolic tiling by all hexagons or by hexagons and squares in the RGCR tiling pattern. □

Theorem 5.9. *RGCR links in thickened surfaces which correspond to the* $[6, 6, 6, 6]$ *tiling are arithmetic.*

Proof. Let H be the doubled complement of the RGCR link shown in Figure 5.4. This link corresponds to the tiling of $\mathbb{H}^2$ by regular right-angled hexagons. In the notation of Chapter 4, $n = 6 = m$ and $k_n = 2 = k_m$. By 5.3, the other RGCR doubled link complements corresponding to the same hexagonal tiling are commensurable to H, so if H has an arithmetic doubled complement then the other doubled link complements corresponding to the hexagonal tiling are as well.

We will find a geometric decomposition of H and use it to show that H and the Whitehead link are commensurable. Consider the decomposition of H shown in Figure 5.4. Each cut-and-pasted semi-truncated generalized bipyramid (which, for brevity, we will refer to as *drums* as in [49, Section 6.8]) consists of two horizontal faces corresponding to the checkerboard surfaces of the original link diagram and 6 vertical faces. We label the horizontal faces F_1, F_2, F_3, and F_4 and label the vertical faces $F_{i,j}$ where i corresponds to the horizontal face and j corresponds to the label on the crossing arc which makes up two of the edges of that vertical face. Under the generalized bipyramid decomposition described in [4] and Chapter 2, we have the following pairs of identifications for the vertical faces of the top row of drums:

$$(F_{1,1}, F_{2,1}), (F_{1,2}, F_{4,2}), (F_{1,3}, F_{2,3}), (F_{1,4}, F_{4,4}), (F_{1,5}, F_{2,5}), (F_{1,6}, F_{4,6}),$$

$$(F_{3,1}, F_{4,1}), (F_{3,2}, F_{2,2}), (F_{3,3}, F_{4,3}), (F_{3,4}, F_{2,4}), (F_{3,5}, F_{4,5}), (F_{3,6}, F_{2,6})$$

and we have the following identifications for the bottom row of drums:

$$(F_{1,1}, F_{4,1}), (F_{1,2}, F_{2,2}), (F_{1,3}, F_{4,3}), (F_{1,4}, F_{2,4}), (F_{1,5}, F_{4,5}), (F_{1,6}, F_{2,6}),$$

$$(F_{3,1}, F_{2,1}), (F_{3,2}, F_{4,2}), (F_{3,3}, F_{2,3}), (F_{3,4}, F_{4,4}), (F_{3,5}, F_{2,5}), (F_{3,6}, F_{4,6})$$

Our choices of diagonal edges for this decomposition (drawn in green) respect these identifications. Observe that each drum decomposes into one ideal right-angled octahedron surrounded by six ideal tetrahedra with dihedral angles $\pi/2, \pi/4$, and $\pi/4$ (see Figures 5.5 and 5.6). We find the dihedral angles on the ideal tetrahedra by noting that each horizontal hexagonal face corresponds to the right-angled tiling of $\mathbb{H}^3$ by hexagons and thus we have $\pi/2$ dihedral angles on the vertical edges

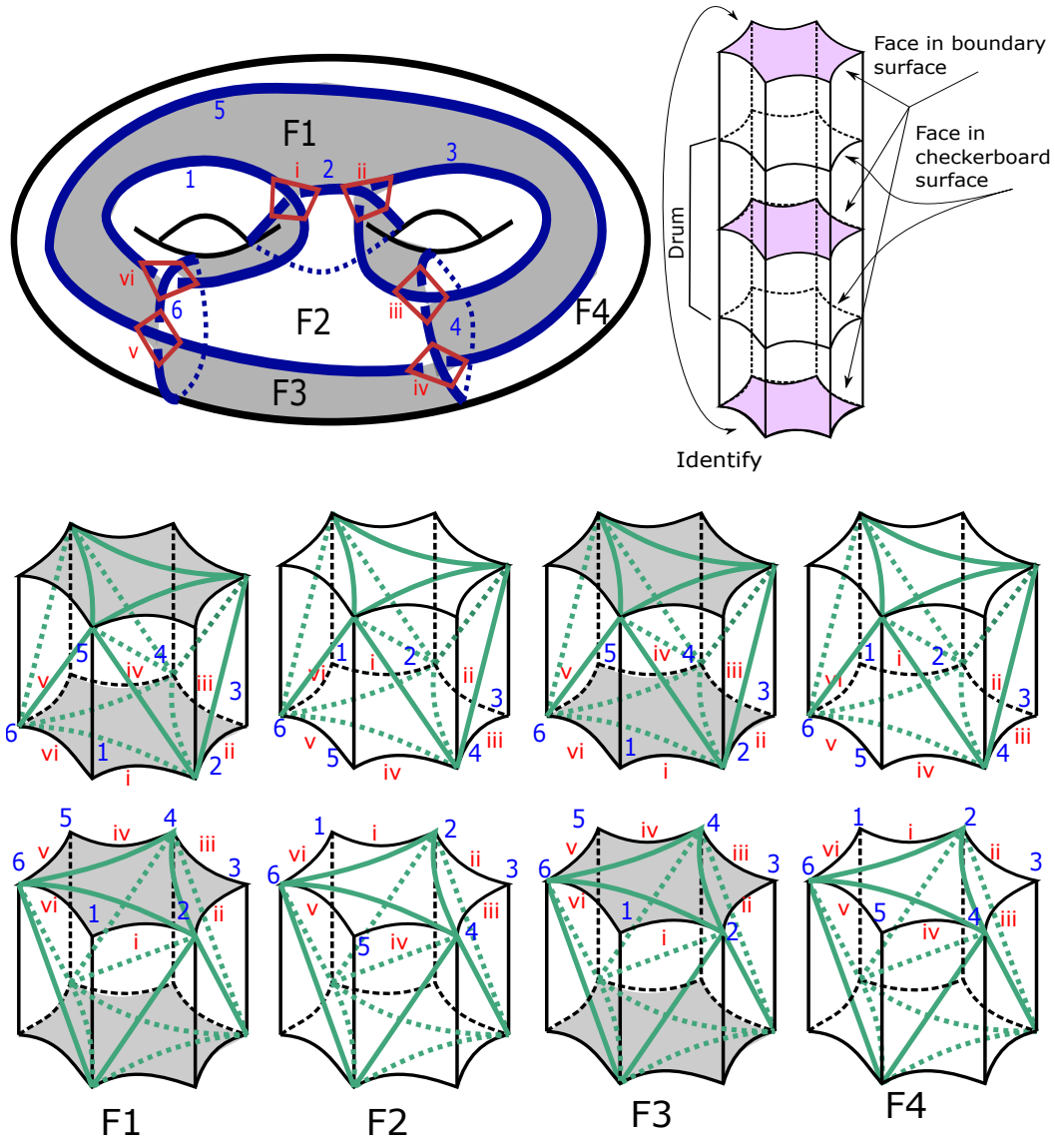

Figure 5.4: A geometric decomposition of an RGCR link with $n = 6 = m$. The strands of the link (which become the ideal vertices of the decomposition) are in blue. The crossing arcs are labeled with roman numerals in red. The face diagonals added to triangulate the doubled complement are shown in green.

shared by the vertical faces of each drum (the edges sharing the same number label within a drum). This forces each crossing arc edge between the horizontal faces and the vertical faces to have full dihedral angle $\pi/4$ in order for the three dihedral angles surrounding an ideal vertex to add to π. We find the dihedral angles on the ideal octahedron by noting that the sum of the dihedral angles corresponding to the same diagonal of the drum decomposition is π.

Next, we will follow the face gluings of the drums to show that the collection of ideal tetrahedra are identified into ideal right-angled octahedra (see Figure 5.7). Each of the 1-6 vertical edges is identified in groups of four (along the top row of drums or the bottom row of drums). As previously discussed, these edges have dihedral angle $\pi/2$, and thus the dihedral angles on the edges directly opposite to them (which lie in the faces corresponding to the checkerboard surfaces) are also $\pi/2$ because opposite dihedral angles in an ideal tetrahedron are equal. The edges of the tetrahedra which are diagonals of the vertical faces of each drum then all have angle $\pi/4$ and are identified according to the face gluing in pairs. This glues 4 tetrahedra about each vertical edge as shown in the example in Figure 5.7, resulting in a right-angled ideal octahedron. Under this decomposition of H, we have 8 octahedra from the 'center' of each drum and 12 from the identifications on the surrounding tetrahedra. Therefore H admits a decomposition into regular ideal octahedra.

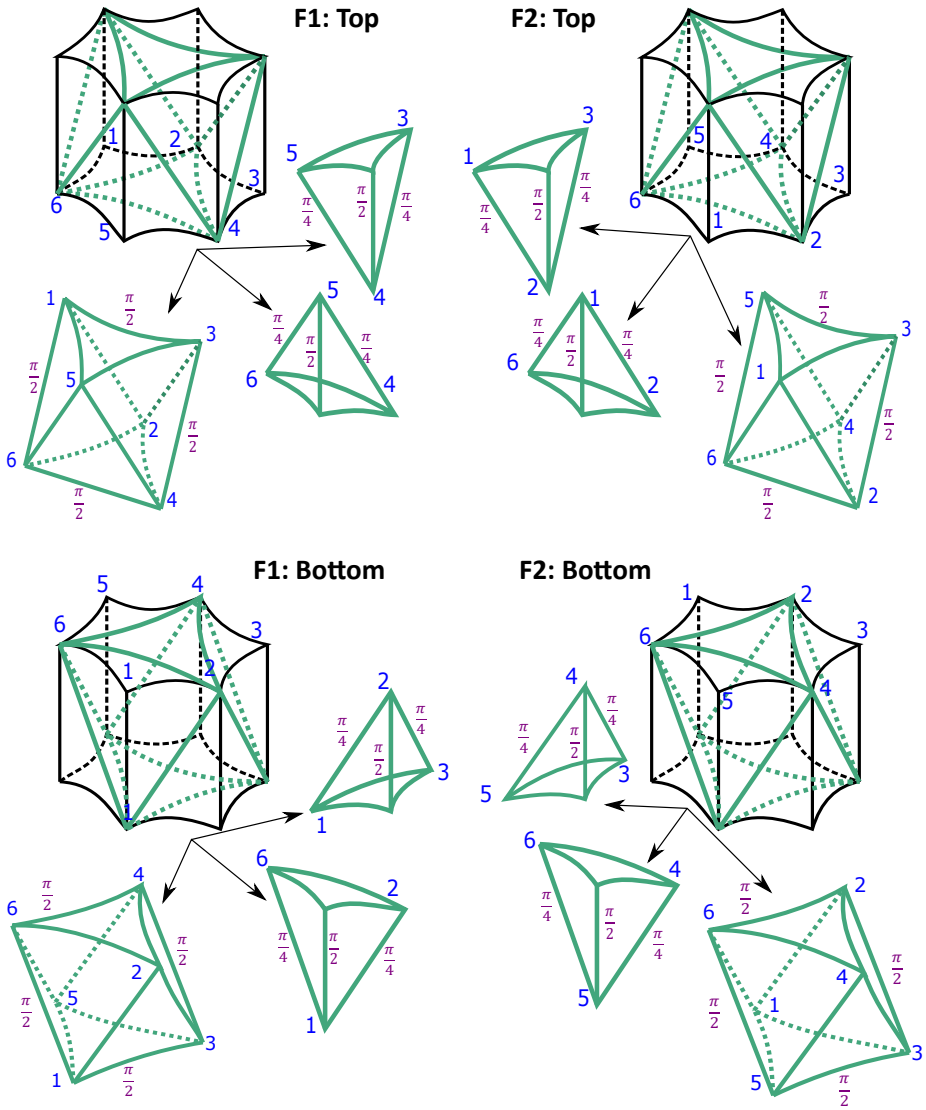

Figure 5.5: The drums forming H each decompose into an ideal regular octahedron and 6 ideal tetrahedra with dihedral angles $\pi/2$, $\pi/4$, and $\pi/4$. Also see Figure 5.6.

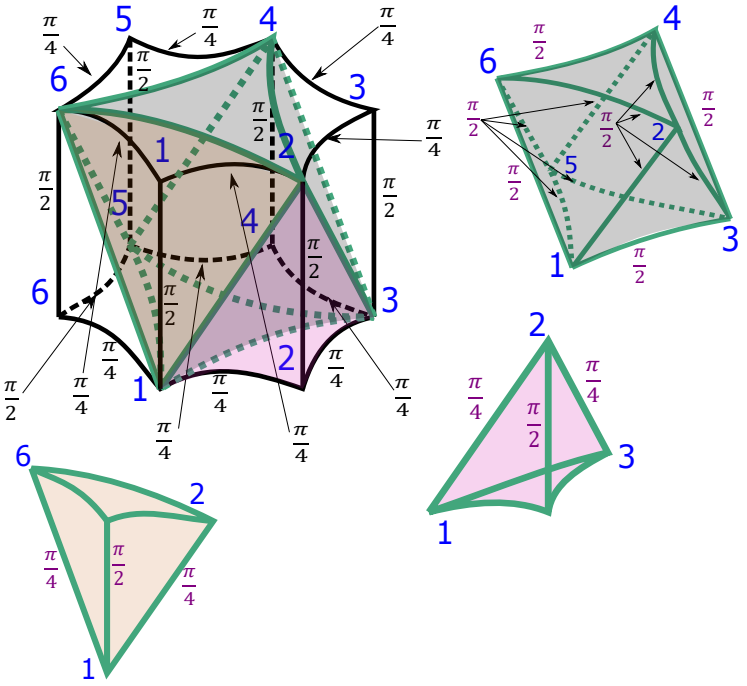

Figure 5.6: A decomposition of one hexagonal drum. The dihedral angles of the original drum are labeled in black. The interior ideal octahedron and 2 of the 6 ideal tetrahedra are shaded.

Both H and the Whitehead link are quotients of a tilings of $\mathbb{H}^3$ by regular ideal octahedra (see [49, Section 6.7]). Therefore, both $\pi_1(H)$ and $\pi_1(S^3\backslash W)$, for W the Whitehead link, are finite index subgroups of the symmetries of the regular octahedral tiling of $\mathbb{H}^3$. The intersection of these fundamental groups, $\pi_1(H)\cap\pi_1(S^3\backslash W)$, has finite index in both groups. This implies that H and the Whitehead link complement are commensurable. The Whitehead link complement is arithmetic, and arithmeticity is a commensurability invariant, so H must be as well. □

Remark 5.10. It is an open question whether links corresponding to the $[4, 6, 4, 6]$ tiling are arithmetic. In Example 5.13 we construct a geometric triangulation for a

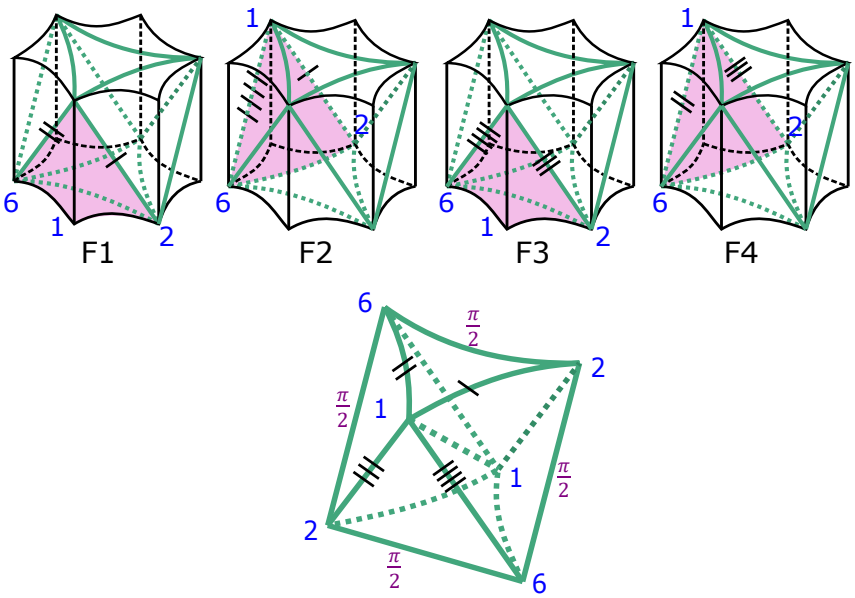

Figure 5.7: Building a right-angled octahedron from the ideal tetrahedra surrounding the octahedra in the 'center' of each drum.

doubled link complement in this commensurability class, S, and use this triangulation to find its volume and invariants of the commensurability class.

We next investigate the *cusp fields* of RGCR link complements.

Definition 5.11. A cusp torus for cusp C in cusped hyperbolic 3-manifold M is conformally equivalent to $\mathbb{C}/\Lambda$ for Λ a complex lattice. The *cusp shape*, p, of C is the ratio of two generators of this Λ. The *cusp field* of C is generated by p and the *cusp field* of M is the field generated by the cusp shapes of all of the cusps in M. The cusp field is independent of the choice of generators for Λ because they differ by the action of $SL_2(\mathbb{Z})$ by Möbius transformations.

We can compute cusp shapes from the cusp triangulation induced by an ideal triangulation of M so the cusp field is contained in the invariant trace field [40]. The

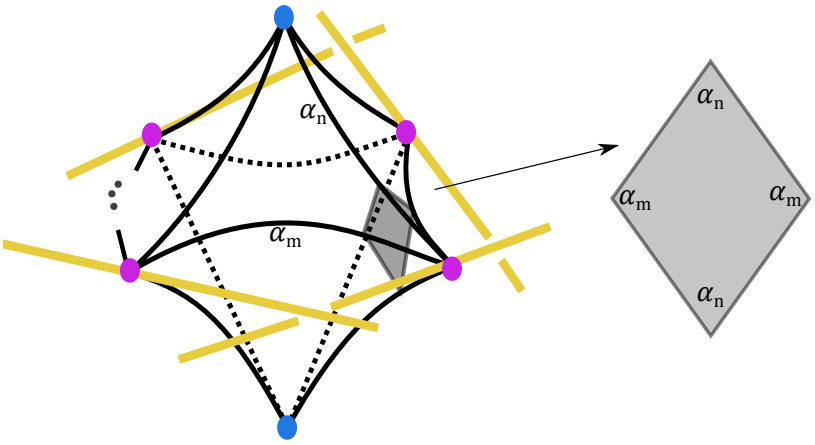

Figure 5.8: Truncating a generalized bipyramid in the decomposition of an RGCR link complement at one of its ideal vertices. The link is shown in yellow, the pink vertices are ideal, and the blue vertices are either ideal or ultra-ideal depending on the genus of the projection surface for the link. The angle α_n is the interior angle of the n-gons and α_m is the interior angle of the m-gons in the link's corresponding tiling.

cusp field is a commensurability invariant and therefore we can determine that two RGCR links must be in different commensurability classes when they have distinct cusp fields.

Lemma 5.12. *The cusp field of an RGCR link complement is* $\mathbb{Q}(i\sin(\alpha_n), \cos(\alpha_n))$ *for* α_n *the interior angle of one of the polygons in the RGCR link's checkerboard surfaces.*

Proof. We can find the cusp shapes of RGCR links by truncating the ideal vertices of their generalized bipyramid decomposition (see Figure 5.8). The truncation face at an ideal vertex is a rhombus with vertices on the edges corresponding to crossing arcs of the link complement and the vertical edges running toward the ultra-ideal apexes of the bipyramids. This means that the rhombus has two interior angles

matching the interior angle of the diagram polygon it is centered upon. We calculate the other two interior angles by using the symmetry of the bipyramid and that the interior angles of the Euclidean rhombus must sum to 2π:

$2\alpha_n + 2x = \pi$, so $x = \alpha_m$.

Normalize the truncation rhombus to have side length 1. Then the cusp shapes are: $\cos(\alpha_n) + i\sin(\alpha_n)$ and

$\cos(\alpha_m) + i\sin(\alpha_m) = \cos(\pi - \alpha_n) + i\sin(\pi - \alpha_n) = -\cos(\alpha_n) + i\sin(\alpha_n)$. So, the cusp field is generated by $\cos(\alpha_n)$ and $i\sin(\alpha_n)$. □

Note that Lemma 5.12 implies that the cusp field of any RGCR link with $n = m$ is $\mathbb{Q}(i)$. RGCR links with only one type of polygon in their diagrams (and therefore $\alpha_n = \alpha_m$) have square fundamental domains for their cusps. More generally, for a given n and m we can calculate the α_n and α_m interior angles. First, we use the hyperbolic law of cosines: $\cosh C = \dfrac{\cos(a)\cos(b) + \cos(c)}{\sin(a)\sin(b)}$ for a hyperbolic triangle with sides A, B, and C, opposite interior angles a, b, and c (see [49, 2.6.8]). Consider the quadrilateral with interior angles $\frac{2\pi}{n}$, $\frac{2\pi}{m}$, and $\pi/2$ in Figure 5.1. This quadrilateral is composed of two hyperbolic triangles (one in an n-gon and the other in an m-gon) sharing an edge. So,

$$\frac{\cos^2(\frac{\alpha_n}{2}) + \cos(\frac{2\pi}{n})}{\sin^2(\frac{\alpha_n}{2})} = \frac{\cos^2(\frac{\alpha_m}{2}) + \cos(\frac{2\pi}{m})}{\sin^2(\frac{\alpha_m}{2})},$$

because both quotients are equal to $\cosh(C)$ for C the length of their shared edge.

Second, $\alpha_n + \alpha_m = \pi$.

An example of the process for calculating the cusp shapes for an RGCR link with distinct n and m is given in Example 5.13. Values of $\cos(\alpha_n)$ and $\sin(\alpha_n)$ for RGCR links with projection surfaces of genus $2-7$ are listed in Table 6.1.

Example 5.13. Consider the RGCR link with square and hexagonal faces shown in Figure 5.9. We will show that links in this commensurability class (which by Proposition 5.3 includes all RGCR links corresponding to the $[4,6,4,6]$ hyperbolic tiling) have cusp field and invariant trace field $\mathbb{Q}(i\sqrt{6})$. Call the doubled complement of this link S.

First we solve for α_4 and α_6 using substitution and trigonometric identities:

$$\frac{\cos^2(\frac{\alpha_4}{2}) + \cos(\frac{2\pi}{4})}{\sin^2(\frac{\alpha_4}{2})} = \frac{\cos^2(\frac{\alpha_6}{2}) + \cos(\frac{2\pi}{6})}{\sin^2(\frac{\alpha_6}{2})}$$

and $\alpha_4 + \alpha_6 = \pi$

$$\implies \frac{\cos^2(\frac{\alpha_4}{2})}{\sin^2(\frac{\alpha_4}{2})} = \frac{\cos^2(\frac{\pi-\alpha_4}{2}) + \frac{1}{2}}{\sin^2(\frac{\pi-\alpha_4}{2})}$$

$$\implies \frac{\cos^2(\frac{\alpha_4}{2})}{\sin^2(\frac{\alpha_4}{2})} = \frac{\sin^2(\frac{\alpha_4}{2}) + \frac{1}{2}}{\cos^2(\frac{\alpha_4}{2})}$$

$$\implies \cot^2(\alpha_4/2) = \tan^2(\alpha_4/2) + \frac{1}{2}\sec^2(\alpha_4/2)$$

$$\implies \csc^2(\alpha_4/2) - 1 - \frac{1}{2}\sec^2(\alpha_4/2) = \tan^2(\alpha_4/2)$$

$$\implies \csc^2(\alpha_4/2) - \frac{1}{2}\sec^2(\alpha_4/2) = \sec^2(\alpha_4/2)$$

$$\implies \cot^2(\alpha_4/2) = 3/2$$

$\implies \alpha_4 = 2\text{arccot}(\sqrt{3/2})$ and $\alpha_6 = \pi - 2\text{arccot}(\sqrt{3/2})$ because $0 < \alpha_4 < \pi/2$.

Using double-angle and forward-inverse identities we see that

$$\sin(\alpha_4) = \sin(2\text{arccot}(\sqrt{3/2})) = \frac{2(\sqrt{3/2})}{(\sqrt{3/2})^2+1} = \frac{2\sqrt{6}}{5},$$

and

$$\cos(\alpha_4) = \cos(2\text{arccot}(\sqrt{3/2})) = 1 - \frac{2}{(\sqrt{3/2})^2+1} = \frac{1}{5}.$$

Applying Lemma 5.12, we see that the cusp field for this commensurability class is $\mathbb{Q}(i\sin(\alpha_4), \cos(\alpha_4)) = \mathbb{Q}(i(\frac{2\sqrt{6}}{5}), \frac{1}{5}) = \mathbb{Q}(i\sqrt{6})$.

In the geometric decomposition of this doubled complement shown in Figure 5.10, each square and hexagonal-face drum consists of two horizontal faces corresponding to the checkerboard surfaces of the original link diagram and 4 or 6 vertical faces. We label the horizontal faces by F_1 through F_8 and once again label the vertical faces $F_{i,j}$ where i corresponds to the horizontal face and j corresponds to the label on the crossing arc which makes up two of the edges of that vertical face. Under the generalized bipyramid decomposition described in Chapter 2, we once again have two sets of drums (a top set and a bottom set) as drawn in Figure 5.10. The top set has the following vertical face identifications under the generalized bipyramid gluing about each crossing:

$(F_{1,1}, F_{8,1}), (F_{1,2}, F_{6,2}), (F_{1,3}, F_{4,3}), (F_{1,4}, F_{2,4}), (F_{2,3}, F_{5,3}), (F_{2,8}, F_{10,8}),$

$(F_{2,7}, F_{3,7}), (F_{2,6}, F_{9,6}), (F_{2,5}, F_{7,5}), (F_{3,12}, F_{4,12}), (F_{3,11}, F_{6,11}), (F_{3,6}, F_{8,6}),$

$(F_{4,7}, F_{10,7}), (F_{4,9}, F_{5,9}), (F_{4,2}, F_{10,2}), (F_{4,8}, F_{5,8}), (F_{5,12}, F_{6,12}), (F_{6,1}, F_{9,1}),$

$(F_{6,10}, F_{7,10}), (F_{6,9}, F_{10,9}), (F_{7,4}, F_{8,4}), (F_{7,11}, F_{8,11}), (F_{8,5}, F_{9,5}), (F_{8,10}, F_{9,10}).$

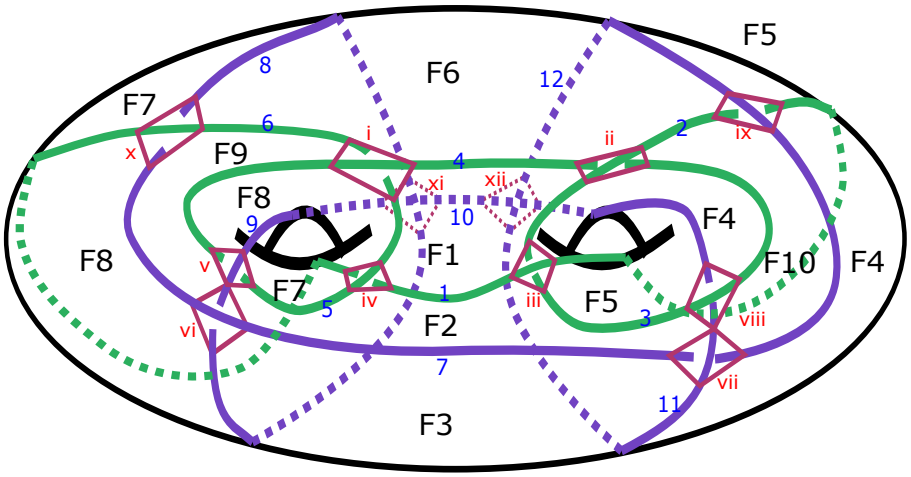

Figure 5.9: An RGCR link corresponding to the $[4, 6, 4, 6]$ tiling. The strands of the link are drawn in purple and green and labeled in blue. Crossing arcs are drawn in red and labeled with roman numerals. The faces of the diagram are labeled F_1-F_{10} in black.

The bottom set of drums have vertical faces identified according to their crossing arcs being on opposite sides of overstrands of the link at each crossing (see Figure 2.6).

Our choices of diagonal edges for this decomposition respect these face identifications. Observe that each square-faced drum decomposes into two 'blocks' consisting of 3 ideal tetrahedra each and the hexagonal-faced drum decomposes into 4 blocks which also decompose into 3 ideal tetrahedra each (see Figure 5.11). Under the symmetry of the drums it suffices for us to consider the tetrahedra from one block in the square-faced drum and two blocks in the hexagonal-faced drum because all other ideal tetrahedra in this geometric ideal triangulation of the manifold will have the same set of dihedral angles as one of the ideal tetrahedra in this set.

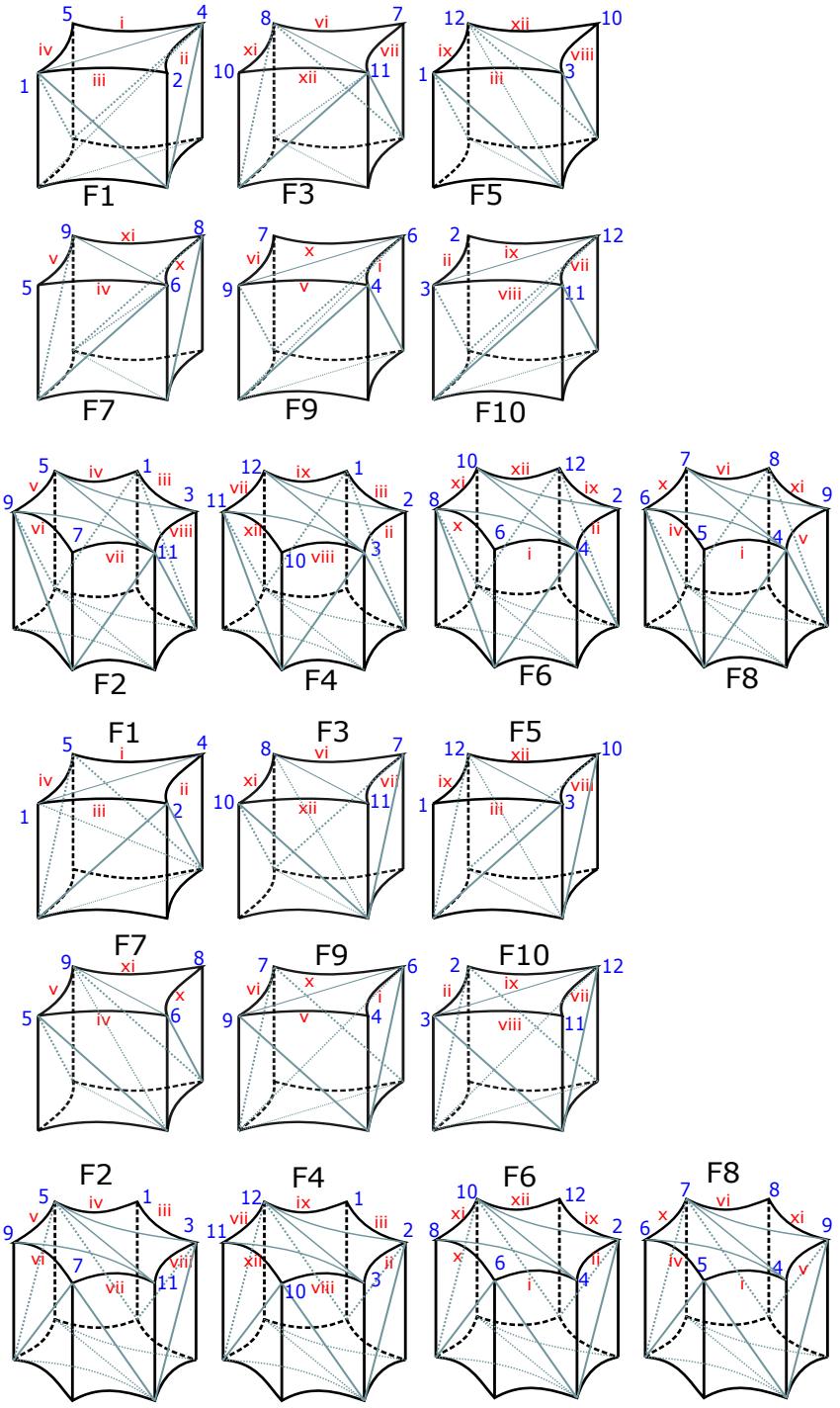

Figure 5.10: A geometric triangulation of the doubled complement of the link in Figure 5.9. Crossing arcs are labeled with roman numerals. The edges in light green triangulate each drum and respect their face identifications.

The dihedral angles of these ideal tetrahedra are given in Figure 5.11. We calculate the angle θ in Figure 5.11 by considering a finite regular hyperbolic hexagon with interior angle α_6. We find the side length, C, of the hexagon (and thus of the squares in the tiling as well) by solving:

$$\cosh(C) = \frac{\cos^2(\alpha_6/2) + \cos(2\pi/6)}{\sin^2(\alpha_6/2)} = \frac{2/5 + 1/2}{3/5} = 3/2$$

$$\implies C = \text{arccosh}(3/2).$$

Then:

$$3/2 = \frac{\cos(\theta) + \cos(\theta)\cos(\alpha_6)}{\sin(\theta)\sin(\alpha_6)} = \frac{\cos(\theta)(4/5)(5)}{\sin(\theta)(2)(\sqrt{6})} = \frac{\sqrt{6}}{3}\cot(\theta)$$

$$\implies \theta = \text{arccot}\left(\frac{3\sqrt{6}}{4}\right).$$

The shapes of these ideal tetrahedra are: $\frac{1}{4}(2 + i\sqrt{6})$ for T_1, $\frac{1}{5}(1 + i\frac{\sqrt{6}}{3})$ for T_2, $\frac{1}{5}(2 + i\sqrt{6})$ for T_3, $\frac{1}{6}(3 + i\sqrt{6})$ for T_4, $3 + i\frac{2\sqrt{6}}{3}$ for T_5, $(\frac{1}{15})(6 + 2i\sqrt{6})$ for T_6, $\frac{1}{5}(2 + i\sqrt{6})$ for T_7, $(\frac{1}{7})(6 + i\sqrt{6})$ for T_8, and $\frac{1}{35}(32 + i4\sqrt{6})$ for T_9. Therefore, the invariant trace field of this commensurability class is $\mathbb{Q}(i\sqrt{6})$.

Example 5.14. We will find a geometric ideal triangulation for the RGCR knot in Figure 3.5. Call the doubled complement K and consider Figures 5.12 and 5.13. We can decompose K into 4 octagonal drums. Each drum then decomposes into

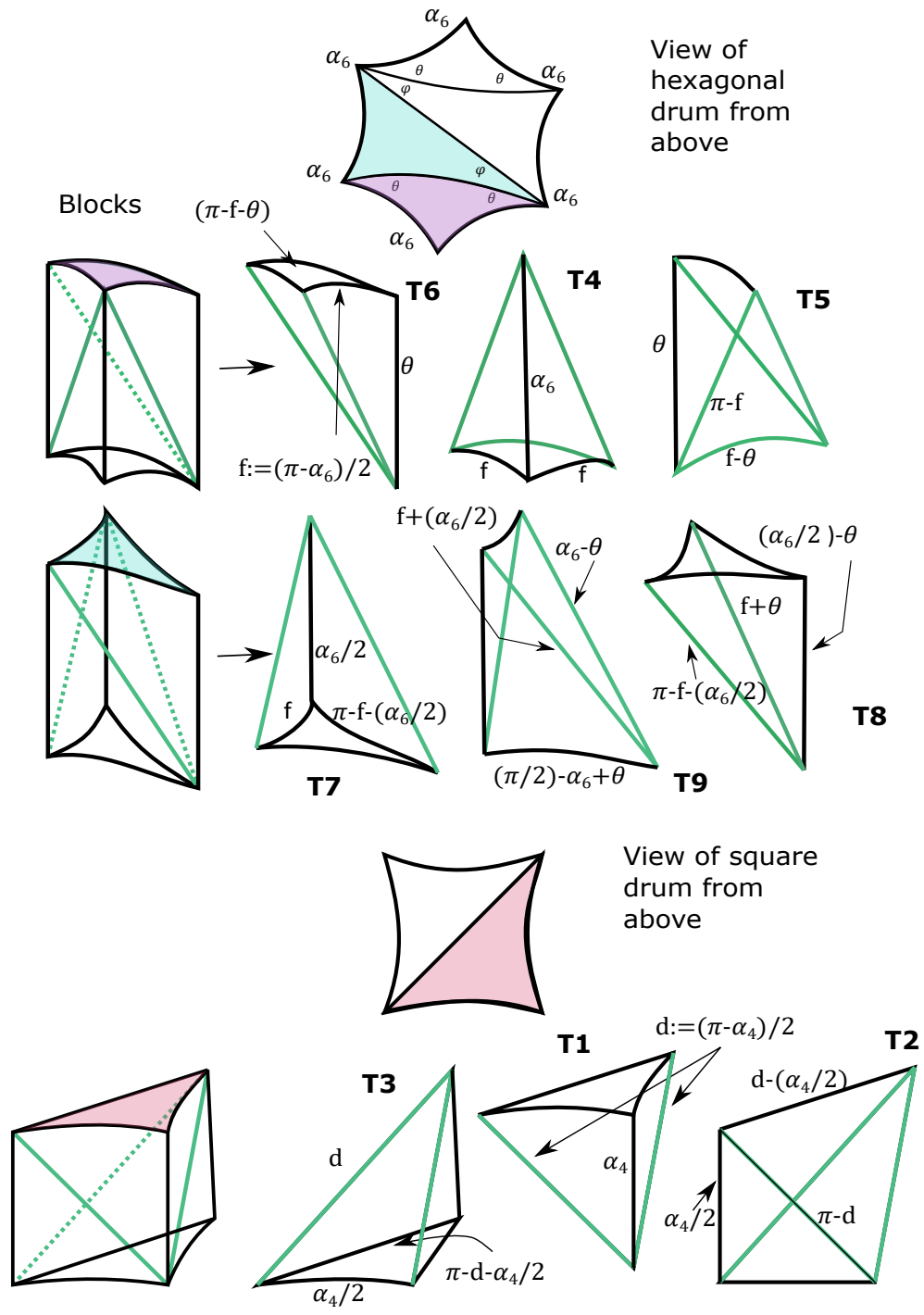

Figure 5.11: The blocks and corresponding ideal tetrahedra in a triangulation of the $[4, 6, 4, 6]$ RGCR doubled link complement, S.

6 blocks, 4 around the side of the drum and a square prism in the middle that subdivides into 2 blocks.

We calculate the interior angle θ for the blocks in the decomposition of K with the same method as in Example 5.13. We find the side length, C, of the right-angled octagons by solving:

$$\cosh(C) = \frac{\cos^2(\pi/4) + \cos(2\pi/8)}{\sin^2(\pi/4)} = \frac{1/2 + \sqrt{2}/2}{1/2} = 1 + \sqrt{2}$$

$$\implies C = \text{arccosh}(1 + \sqrt{2}).$$

Then:

$$1 + \sqrt{2} = \frac{\cos(\theta) + \cos(\theta)\cos(\pi/2)}{\sin(\theta)\sin(\pi/2)} = \cot(\theta)$$

$$\implies \theta = \text{arccot}(1 + \sqrt{2}).$$

We once again use the symmetry of the blocks to reduce the number of distinct ideal tetrahedra we consider. The dihedral angles of the ideal tetrahedra that the blocks decompose into are shown in Figure 5.13. There are 6 distinct ideal tetrahedra in this triangulation, labeled T_1 to T_6 in Figure 5.13. The shapes of these ideal tetrahedra are: $i(-1 + \sqrt{2})$ for T_1, 1 for T_2, $\frac{1}{2}(1 + \sqrt{2} + i)$ for T_3, i for T_4, $\frac{1}{2}(-\sqrt{2} + i\sqrt{2})$ for T_5, and $\frac{1}{2}(\sqrt{2} + i(2 - \sqrt{2})$ for T_6. So, applying [40, Theorem 2.4] again, we see that K has invariant trace field $\mathbb{Q}(i, \sqrt{2})$.

We doubled the complement of a knot to build K, so K has two cusps. A fundamental domain for one of the cusps is in Figure 5.12. Using that the tiles are square ($n = m = 8$ in this example), we see that the cusp field of K is $\mathbb{Q}(i)$.

Finding geometric ideal triangulations of a finite volume cusped hyperbolic 3-manifold M is an independently interesting problem. Families of link complements have been found to admit geometric ideal triangulations (for example, see [23]) and it was previously thought that any such M would admit a geometric ideal triangulation as a consequence of Epstein and Penner's work on canonical decompositions [17]. However, the problem has turned out to be more complex. Petronio conjectured that every cusped hyperbolic 3-manifold admits at least one geometric triangulation [42, Conjecture 2.3]. In [19], Futer, Hamilton, and Hoffman strengthen this statement. They conjecture that any such M admits infinitely many geometric ideal triangulations and proved that a cusped hyperbolic 3-manifold admits a finite cover with infinitely many geometric ideal triangulations [19, Conjecture 1.1 and Theorem 1.2].

We can also use geometric ideal triangulations to find the volumes of the links in our examples. Adams, Calderon, and Mayer described a method for calculating the volume of link complements in thickened surfaces with regular faces by calculating the volumes of their generalized bipyramids using Ushijima's formula for the volume of generalized hyperbolic tetrahedra [51]. If our doubled link complement has a geometric triangulation then we have another method for calculating

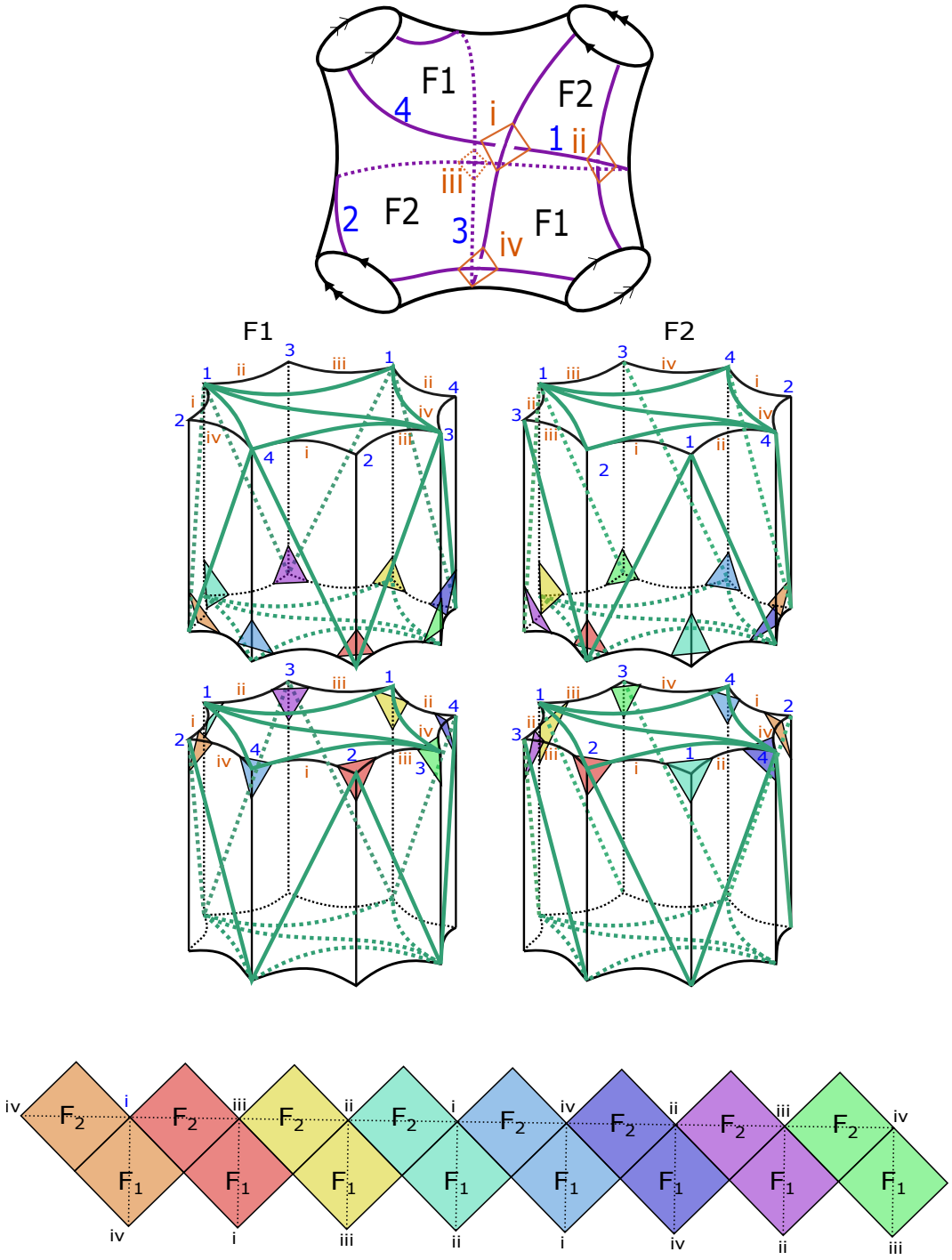

Figure 5.12: A geometric decomposition of the doubled complement of the RGCR knot previously shown in Figure 3.5. Below the drums of the decomposition is a fundamental domain for the boundary torus of one of the doubled complement's two cusps. We construct this fundamental domain by truncating the set of ideal vertices which correspond to the same component of the link and identifying the truncation faces according to the face pairing in the decomposition. The crossing arcs and strands follow the same coloring and labeling conventions of the previous examples, red for crossing arcs and blue for strands of the link. The truncation faces have a rainbow coloring.

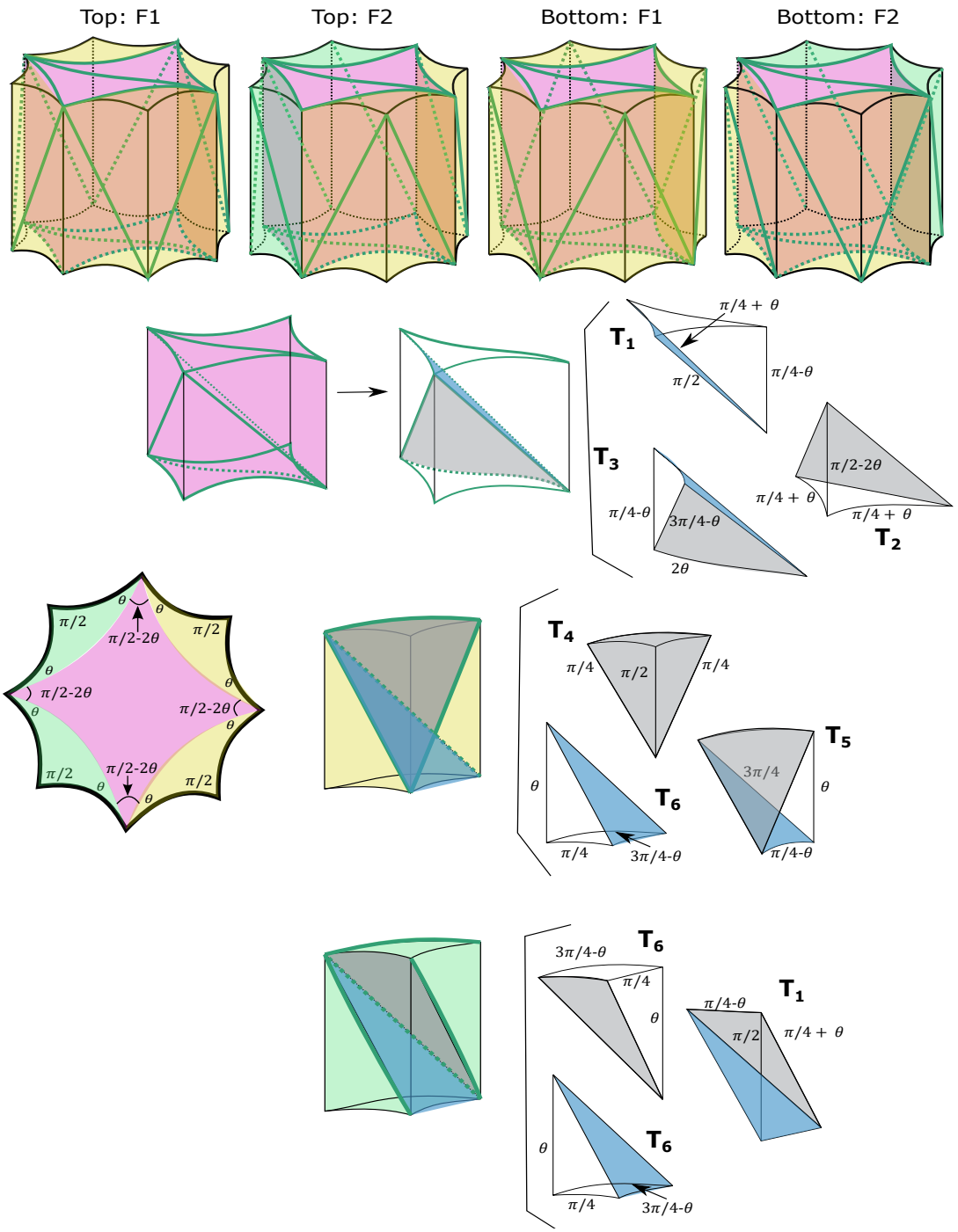

Figure 5.13: The ideal tetrahedra in a geometric ideal triangulation of K. The square prism in the center of each drum is shaded pink while the blocks around the 'side' of each drum are shaded yellow or light green depending on the pattern of their face diagonals. The view from infinity of the top F_2 drum is shown on the left with its dihedral angles labeled. The blue and gray shading indicates the faces the ideal tetrahedra are glued along to form the blocks.

these volumes, without requiring the generalized volume formulas. Namely, the volume of the complement is half of the sum of the volumes of the ideal tetrahedra forming the double. The volume of an ideal tetrahedron with angles α, β, γ is $\Lambda(\alpha) + \Lambda(\beta) + \Lambda(\gamma)$ where Λ is the *Lobachevsky function*,

$$\Lambda(\theta) = -\int_0^\theta \log|2\sin(u)|du$$

(see [49, Theorem 7.2.1] and [45, Theorem 9.3]). For S, in Figure 5.9, the square-faced drums have volume:

$$2[3\Lambda(d) + 2\Lambda\left(\frac{\alpha_4}{2}\right) + \Lambda(\pi - d - \left(\frac{\alpha_4}{2}\right)) + \Lambda(\alpha_4) + \Lambda(d - \left(\frac{\alpha_4}{2}\right)) + \Lambda(\pi - d)]$$
$$\approx 4.6695$$

and the hexagonal-faced drums have volume:

$$2(4\Lambda(f) + \Lambda(\alpha_6) + 2\Lambda(\theta) + \Lambda(\pi - f) + \Lambda(f - \theta) + \Lambda(\pi - f - \theta) + \Lambda\left(\frac{\alpha_6}{2}\right)$$
$$+2\Lambda(\pi - f - \frac{\alpha_6}{2}) + \Lambda(\alpha_6 - \theta) + \Lambda(f + \frac{\alpha_6}{2}) + \Lambda(\frac{\pi}{2} - \alpha_6 + \theta) + \Lambda(f + \theta) + \Lambda(\frac{\alpha_6}{2} - \theta))$$
$$\approx 8.5423.$$

Hence the link in Figure 5.9 has volume: ≈ 62.1861. The volumes of the octagonal drums for the RGCR knot in Figure 3.5 are ≈ 13.35078 so the volume of the RGCR knot is ≈ 26.7015. The volume of the regular ideal octahedron is $v_{oct} \approx 3.6638$.

Therefore the link in Figure 5.4 in the thickened genus two surface has volume $10v_{oct} \approx 36.6386$.

Future directions for this work include generalizing the triangulations shown in Figures 5.5 and 5.10 for all RGCR links and determining the arithmeticity of the $[4, 6, 4, 6]$ links.

CHAPTER 6

TABLE

Table 6.1: The tilings corresponding to RGCR links on projection surfaces of genus $2-7$. We list the possible values of m, n, k_m, k_n, $\cos(\alpha_n)$, and $\sin(\alpha_n)$ for each projection surface. These values are calculated from the bounds and Equations 4.1 and 4.2 in Chapter 4.

Genus	**m**	**n**	$\mathbf{k_m}$	$\mathbf{k_n}$	**cos**$(\alpha_\mathbf{n})$	**sin**$(\alpha_\mathbf{n})$
2	5	4	8	10	$\frac{1}{11}(-3+2\sqrt{5})$	$\frac{4\sqrt{3+\sqrt{5}}}{7+\sqrt{5}}$
2	6	4	4	6	$\frac{1}{5}$	$\frac{2\sqrt{6}}{5}$
2	7	3	12	28	$\frac{1+2\sin(3\pi/14)}{3+2\sin(3\pi/14)}$	$\frac{2\sqrt{2(1+\sin(3\pi/14))}}{3+2\sin(3\pi/14)}$
2	8	3	6	16	$\frac{1}{7}(1+2\sqrt{2})$	$\frac{2\sqrt{2+\sqrt{2}}}{3+\sqrt{2}}$
2	8	4	2	4	$\frac{1}{7}(-1+2\sqrt{2})$	$\frac{2\sqrt{10+\sqrt{2}}}{7}$
2	9	3	4	12	$\frac{1+2\cos(2\pi/9)}{3+2\cos(2\pi/9)}$	$\frac{4\cos(\pi/9)}{3+2\cos(2\pi/9)}$
2	10	3	3	10	$\frac{1}{11}(4+\sqrt{5})$	$\frac{2\sqrt{2(5+\sqrt{5})}}{7+\sqrt{5}}$
2	10	5	1	2	$\frac{1}{11}(4-\sqrt{5})$	$\frac{2\sqrt{5+2\sqrt{5}}}{4+\sqrt{5}}$
2	12	3	2	8	$\frac{\sqrt{3}}{3}$	$\frac{2\sqrt{2+\sqrt{3}}}{3+\sqrt{3}}$
2	12	4	1	3	$\frac{1}{13}(-3+4\sqrt{3})$	$\frac{2\sqrt{2(2+\sqrt{3})}}{4+\sqrt{3}}$

Table 6.1 – continued from previous page

Genus	**m**	**n**	$\mathbf{k_m}$	$\mathbf{k_n}$	$\mathbf{cos}(\alpha_\mathbf{n})$	$\mathbf{sin}(\alpha_\mathbf{n})$
2	18	3	1	6	$\frac{1+2\cos(\pi/9)}{3+2\cos(\pi/9)}$	$\frac{2\sqrt{2(1+\cos(\pi/9))}}{3+2\cos(\pi/9)}$
2	8	8	1	1	0	1
2	6	6	2	2	0	1
2	5	5	4	4	0	1
3	5	4	16	20	$\frac{1}{11}(-3+2\sqrt{5})$	$\frac{4\sqrt{3+\sqrt{5}}}{7+\sqrt{5}}$
3	6	4	8	12	$\frac{1}{5}$	$\frac{2\sqrt{6}}{5}$
3	6	5	5	6	$\frac{1}{19}(8-3\sqrt{5})$	$\frac{2\sqrt{6(3+\sqrt{5})}}{9+\sqrt{5}}$
3	7	3	24	56	$\frac{1+2\sin(3\pi/14)}{3+2\sin(3\pi/14)}$	$\frac{2\sqrt{2(1+\sin(3\pi/14))}}{3+2\sin(3\pi/14)}$
3	8	3	12	32	$\frac{1}{7}(1+2\sqrt{2})$	$\frac{2\sqrt{2+\sqrt{2}}}{3+\sqrt{2}}$
3	8	4	4	8	$\frac{1}{7}(-1+2\sqrt{2})$	$\frac{2\sqrt{10+\sqrt{2}}}{7}$
3	9	3	8	24	$\frac{1+2\cos(2\pi/9)}{3+2\cos(2\pi/9)}$	$\frac{4\cos(\pi/9)}{3+2\cos(2\pi/9)}$
3	9	6	2	3	$\frac{-1+2\cos(2\pi/9)}{5+2\cos(2\pi/9)}$	$\frac{2\sqrt{6(1+\cos(2\pi/9))}}{5+2\cos(2\pi/9)}$
3	10	3	6	20	$\frac{1}{11}(4+\sqrt{5})$	$\frac{2\sqrt{2(5+\sqrt{5})}}{7+\sqrt{5}}$
3	10	5	2	4	$\frac{1}{11}(4-\sqrt{5})$	$\frac{2\sqrt{5+2\sqrt{5}}}{4+\sqrt{5}}$
3	12	3	4	16	$\frac{\sqrt{3}}{3}$	$\frac{2\sqrt{2+\sqrt{3}}}{3+\sqrt{3}}$
3	12	4	2	6	$\frac{1}{13}(-3+4\sqrt{3})$	$\frac{2\sqrt{2(2+\sqrt{3})}}{4+\sqrt{3}}$
3	14	3	3	14	$\frac{1+2\cos(\pi/7)}{3+2\cos(\pi/7))}$	$\frac{2\sqrt{2(1+\cos(\pi/7))}}{3+2\cos(\pi/7)}$
3	14	7	1	2	$\frac{\cos(\pi/7)-\sin(3\pi/14)}{2+\cos(\pi/7)+\sin(3\pi/14)}$	$\frac{2\sqrt{(1+\cos(\pi/7))(1+\sin(3\pi/14))}}{2+\cos(\pi/7)+\sin(3\pi/14)}$

Table 6.1 – continued from previous page

Genus	**m**	**n**	$\mathbf{k_m}$	$\mathbf{k_n}$	$\mathbf{cos}(\alpha_\mathbf{n})$	$\mathbf{sin}(\alpha_\mathbf{n})$
3	18	3	2	12	$\frac{1+2\cos(\pi/9)}{3+2\cos(\pi/9)}$	$\frac{2\sqrt{2(1+\cos(\pi/9))}}{3+2\cos(\pi/9)}$
3	20	4	1	5	$\frac{\sqrt{2(5+\sqrt{5})}}{8+\sqrt{2(5+\sqrt{5})}}$	$\frac{4\sqrt{4+\sqrt{2(5+\sqrt{5})}}}{8+\sqrt{2(5+\sqrt{5})}}$
3	30	3	1	10	$\frac{1+2\cos(\pi/15)}{3+2\cos(\pi/15)}$	$\frac{4\cos(\pi/30)}{3+2\cos(\pi/15)}$
3	12	12	1	1	0	1
3	8	8	2	2	0	1
3	6	6	4	4	0	1
3	5	5	8	8	0	1
4	5	4	24	30	$\frac{1}{11}(-3+2\sqrt{5})$	$\frac{4\sqrt{3+\sqrt{5}}}{7+\sqrt{5}}$
4	6	4	12	18	$\frac{1}{5}$	$\frac{2\sqrt{6}}{5}$
4	7	3	36	84	$\frac{1+2\sin(3\pi/14)}{3+2\sin(3\pi/14)}$	$\frac{2\sqrt{2(1+\sin(3\pi/14))}}{3+2\sin(3\pi/14)}$
4	7	4	8	14	$\frac{\sin(3\pi/14)}{2+\sin(3\pi/14)}$	$\frac{2\sqrt{1+\sin(3\pi/14)}}{2+\sin(3\pi/14)}$
4	8	3	18	48	$\frac{1}{7}(1+2\sqrt{2})$	$\frac{2\sqrt{2+\sqrt{2}}}{3+\sqrt{2}}$
4	8	4	6	12	$\frac{1}{7}(-1+2\sqrt{2})$	$\frac{2\sqrt{10+\sqrt{2}}}{7}$
4	9	3	12	36	$\frac{1+2\cos(2\pi/9)}{3+2\cos(2\pi/9)}$	$\frac{4\cos(\pi/9)}{3+2\cos(2\pi/9)}$
4	10	3	9	30	$\frac{1}{11}(4+\sqrt{5})$	$\frac{2\sqrt{2(5+\sqrt{5})}}{7+\sqrt{5}}$
4	10	4	4	10	$\frac{1}{19}(1+2\sqrt{5})$	$\frac{4\sqrt{5+\sqrt{5}}}{9+\sqrt{5}}$
4	10	5	3	6	$\frac{1}{11}(4-\sqrt{5})$	$\frac{2\sqrt{5+2\sqrt{5}}}{4+\sqrt{5}}$
4	12	3	6	24	$\frac{\sqrt{3}}{3}$	$\frac{2\sqrt{2+\sqrt{3}}}{3+\sqrt{3}}$

Table 6.1 – continued from previous page

Genus	**m**	**n**	$\mathbf{k_m}$	$\mathbf{k_n}$	$\mathbf{cos}(\alpha_\mathbf{n})$	$\mathbf{sin}(\alpha_\mathbf{n})$
4	12	4	3	9	$\frac{1}{13}(-3+4\sqrt{3})$	$\frac{2\sqrt{2(2+\sqrt{3})}}{4+\sqrt{3}}$
4	12	6	2	4	$\frac{1}{11}(-4+3\sqrt{3})$	$\frac{2\sqrt{3(2+\sqrt{3})}}{5+\sqrt{3}}$
4	15	3	4	20	$\frac{1+2\cos(2\pi/15)}{3+2\cos(2\pi/15)}$	$\frac{4\cos(\pi/15)}{3+2\cos(2\pi/15)}$
4	16	4	2	8	$\frac{\cos(\pi/8)}{2+\cos(\pi/8)}$	$\frac{2\sqrt{1+\cos(\pi/8)}}{2+\cos(\pi/8)}$
4	18	3	3	18	$\frac{1+2\cos(\pi/9)}{3+2\cos(\pi/9)}$	$\frac{2\sqrt{2(1+\cos(\pi/9))}}{3+2\cos(\pi/9)}$
4	18	9	1	2	$\frac{\cos(\pi/9)-\cos(2\pi/9)}{2+\cos(\pi/9)+\cos(2\pi/9)}$	$\frac{\sqrt{5+6\cos(\pi/9)+4\cos(2\pi/9)}}{2+\cos(\pi/9)+\cos(2\pi/9)}$
4	24	3	2	16	$\frac{2+\sqrt{2}+\sqrt{6}}{6+\sqrt{2}+\sqrt{6}}$	$\frac{2\sqrt{2(4+\sqrt{2}+\sqrt{6})}}{6+\sqrt{2}+\sqrt{6}}$
4	28	4	1	7	$\frac{\cos(\pi/14)}{2+\cos(\pi/14)}$	$\frac{2\sqrt{1+\cos(\pi/14)}}{2+\cos(\pi/14)}$
4	42	3	1	14	$\frac{(1/2)+\cos(\pi/21)}{(3/2)+\cos(\pi/21)}$	$\frac{4\cos(\pi/42)}{3+2\cos(\pi/21)}$
4	16	16	1	1	0	1
4	10	10	2	2	0	1
4	8	8	3	3	0	1
4	7	7	4	4	0	1
4	6	6	6	6	0	1
4	5	5	12	12	0	1
5	5	4	32	40	$\frac{1}{11}(-3+2\sqrt{5})$	$\frac{4\sqrt{3+\sqrt{5}}}{7+\sqrt{5}}$
5	6	4	16	24	$\frac{1}{5}$	$\frac{2\sqrt{6}}{5}$
5	6	5	10	12	$\frac{1}{19}(8-3\sqrt{5})$	$\frac{2\sqrt{6(3+\sqrt{5})}}{9+\sqrt{5}}$

Table 6.1 – continued from previous page

Genus	**m**	**n**	$\mathbf{k_m}$	$\mathbf{k_n}$	$\mathbf{cos}(\alpha_\mathbf{n})$	$\mathbf{sin}(\alpha_\mathbf{n})$
5	7	3	48	112	$\frac{1+2\sin(3\pi/14)}{3+2\sin(3\pi/14)}$	$\frac{2\sqrt{2(1+\sin(3\pi/14))}}{3+2\sin(3\pi/14)}$
5	7	6	6	7	$\frac{-1+2\sin(3\pi/14)}{5+2\sin(3\pi/14)}$	$\frac{2\sqrt{6(1+\sin(3\pi/14))}}{5+2\sin(3\pi/14)}$
5	8	3	24	64	$\frac{1}{7}(1+2\sqrt{2})$	$\frac{2\sqrt{2+\sqrt{2}}}{3+\sqrt{2}}$
5	8	4	8	16	$\frac{1}{7}(-1+2\sqrt{2})$	$\frac{2\sqrt{10+\sqrt{2}}}{7}$
5	9	3	16	48	$\frac{1+2\cos(2\pi/9)}{3+2\cos(2\pi/9)}$	$\frac{4\cos(\pi/9)}{3+2\cos(2\pi/9)}$
5	9	6	4	6	$\frac{-1+2\cos(2\pi/9)}{5+2\cos(2\pi/9)}$	$\frac{2\sqrt{6(1+\cos(2\pi/9))}}{5+2\cos(2\pi/9)}$
5	10	3	12	40	$\frac{1}{11}(4+\sqrt{5})$	$\frac{2\sqrt{2(5+\sqrt{5})}}{7+\sqrt{5}}$
5	10	5	4	8	$\frac{1}{11}(4-\sqrt{5})$	$\frac{2\sqrt{5+2\sqrt{5}}}{4+\sqrt{5}}$
5	12	3	8	32	$\frac{\sqrt{3}}{3}$	$\frac{2\sqrt{2+\sqrt{3}}}{3+\sqrt{3}}$
5	12	4	4	12	$\frac{1}{13}(-3+4\sqrt{3})$	$\frac{2\sqrt{2(2+\sqrt{3})}}{4+\sqrt{3}}$
5	14	3	6	28	$\frac{1+2\cos(\pi/7)}{3+2\cos(\pi/7))}$	$\frac{2\sqrt{2(1+\cos(\pi/7))}}{3+2\cos(\pi/7)}$
5	14	7	2	4	$\frac{\cos(\pi/7)-\sin(3\pi/14)}{2+\cos(\pi/7)+\sin(3\pi/14)}$	$\frac{2\sqrt{(1+\cos(\pi/7))(1+\sin(3\pi/14))}}{2+\cos(\pi/7)+\sin(3\pi/14)}$
5	15	6	2	5	$\frac{-1+2\cos(2\pi/15)}{5+2\cos(2\pi/15)}$	$\frac{2\sqrt{6(1+\cos(2\pi/15))}}{5+2\cos(2\pi/15)}$
5	18	3	4	24	$\frac{1+2\cos(\pi/9)}{3+2\cos(\pi/9)}$	$\frac{2\sqrt{2(1+\cos(\pi/9))}}{3+2\cos(\pi/9)}$
5	20	4	2	10	$\frac{\sqrt{2(5+\sqrt{5})}}{8+\sqrt{2(5+\sqrt{5})}}$	$\frac{4\sqrt{4+\sqrt{2(5+\sqrt{5})}}}{8+\sqrt{2(5+\sqrt{5})}}$
5	22	3	3	22	$\frac{1+2\cos(\pi/11)}{3+2\cos(\pi/11)}$	$\frac{4\cos(\pi/22)}{3+2\cos(\pi/11)}$
5	22	11	1	2	$\frac{\cos(\pi/11)-\cos(2\pi/11)}{2+\cos(\pi/11)+\cos(2\pi/11)}$	$\frac{2\sqrt{(1+\cos(\pi/11))(1+\cos(2\pi/11))}}{2+\cos(\pi/11)+\cos(2\pi/11)}$
5	24	8	1	3	$\frac{\sqrt{2}(-1+\sqrt{3})}{8+3\sqrt{2}+\sqrt{6}}$	$\frac{4\sqrt{5+3\sqrt{2}+\sqrt{3}+\sqrt{6}}}{8+3\sqrt{2}+\sqrt{6}}$

Table 6.1 – continued from previous page

Genus	**m**	**n**	$\mathbf{k_m}$	$\mathbf{k_n}$	$\mathbf{cos}(\alpha_\mathbf{n})$	$\mathbf{sin}(\alpha_\mathbf{n})$
5	30	3	2	20	$\frac{1+2\cos(\pi/15)}{3+2\cos(\pi/15)}$	$\frac{4\cos(\pi/30)}{3+2\cos(\pi/15)}$
5	30	5	1	6	$\frac{1-\sqrt{5}+4\cos(\pi/15)}{7+\sqrt{5}+4\cos[\pi/15)]}$	$\frac{4\sqrt{(3+\sqrt{5})(1+\cos(\pi/15))}}{7+\sqrt{5}+4\cos(\pi/15)}$
5	36	4	1	9	$\frac{\cos(\pi/18)}{2+\cos(\pi/18)}$	$\frac{2\sqrt{1+\cos(\pi/18)}}{2+\cos(\pi/18)}$
5	54	3	1	18	$\frac{1+2\cos(\pi/27)}{3+2\cos(\pi/27)}$	$\frac{4\cos(\pi/54)}{3+2\cos(\pi/27)}$
5	20	20	1	1	0	1
5	12	12	2	2	0	1
5	8	8	4	4	0	1
5	6	6	8	8	0	1
5	5	5	16	16	0	1
6	5	4	40	50	$\frac{1}{11}(-3+2\sqrt{5})$	$\frac{4\sqrt{3+\sqrt{5}}}{7+\sqrt{5}}$
6	6	4	20	30	$\frac{1}{5}$	$\frac{2\sqrt{6}}{5}$
6	7	3	60	140	$\frac{1+2\sin(3\pi/14)}{3+2\sin(3\pi/14)}$	$\frac{2\sqrt{2(1+\sin(3\pi/14))}}{3+2\sin(3\pi/14)}$
6	8	3	30	80	$\frac{1}{7}(1+2\sqrt{2})$	$\frac{2\sqrt{2+\sqrt{2}}}{3+\sqrt{2}}$
6	8	4	10	20	$\frac{1}{7}(-1+2\sqrt{2})$	$\frac{2\sqrt{10+\sqrt{2}}}{7}$
6	8	6	6	8	$\frac{1}{23}(-7+6\sqrt{2})$	$\frac{2\sqrt{3(2+\sqrt{2})}}{5+\sqrt{2}}$
6	9	3	20	60	$\frac{1+2\cos(2\pi/9)}{3+2\cos(2\pi/9)}$	$\frac{4\cos(\pi/9)}{3+2\cos(2\pi/9)}$
6	9	4	8	18	$\frac{\cos(2\pi/9)}{2+\cos(2\pi/9)}$	$\frac{2\sqrt{1+\cos(2\pi/9)}}{2+\cos(2\pi/9)}$
6	10	3	15	50	$\frac{1}{11}(4+\sqrt{5})$	$\frac{2\sqrt{2(5+\sqrt{5})}}{7+\sqrt{5}}$

Table 6.1 – continued from previous page

Genus	**m**	**n**	$\mathbf{k_m}$	$\mathbf{k_n}$	$\mathbf{cos}(\alpha_\mathbf{n})$	$\mathbf{sin}(\alpha_\mathbf{n})$
6	10	5	5	10	$\frac{1}{11}(4-\sqrt{5})$	$\frac{2\sqrt{5+2\sqrt{5}}}{4+\sqrt{5}}$
6	11	3	12	44	$\frac{1+2\cos(2\pi/11)}{3+2\cos(2\pi/11)}$	$\frac{4\cos(\pi/11)}{3+2\cos(2\pi/11)}$
6	12	3	10	40	$\frac{\sqrt{3}}{3}$	$\frac{2\sqrt{2+\sqrt{3}}}{3+\sqrt{3}}$
6	12	4	5	15	$\frac{1}{13}(-3+4\sqrt{3})$	$\frac{2\sqrt{2(2+\sqrt{3})}}{4+\sqrt{3}}$
6	14	4	4	14	$\frac{\cos(\pi/7)}{2+\cos(\pi/7)}$	$\frac{2\sqrt{1+\cos(\pi/7)}}{2+\cos(\pi/7)}$
6	15	10	2	3	$-\frac{1+\sqrt{5}-4\cos(2\pi/15)}{9+\sqrt{5}+4\cos(2\pi/15)}$	$\frac{4\sqrt{(5+\sqrt{5})(1+\cos(2\pi/15))}}{9+\sqrt{5}+4\cos(2\pi/15)}$
6	16	3	6	32	$\frac{1+2\cos(\pi/8)}{3+2\cos(\pi/8)}$	$\frac{2\sqrt{2(1+\cos(\pi/8))}}{3+2\cos(\pi/8)}$
6	16	8	2	4	$\frac{-\sqrt{2}/2+\cos(\pi/8)}{2+\sqrt{2}/2+\cos(\pi/8)}$	$\frac{2\sqrt{2(2+\sqrt{2})(1+\cos(\pi/8))}}{4+\sqrt{2}+2\cos(\pi/8)}$
6	18	3	5	30	$\frac{1+2\cos(\pi/9)}{3+2\cos(\pi/9)}$	$\frac{2\sqrt{2(1+\cos(\pi/9))}}{3+2\cos(\pi/9)}$
6	18	6	2	6	$\frac{-1+2\cos(\pi/9)}{5+2\cos(\pi/9)}$	$\frac{2\sqrt{6(1+\cos(\pi/9))}}{5+2\cos(\pi/9)}$
6	20	5	2	8	$\frac{1-\sqrt{5}+\sqrt{2(5+\sqrt{5})}}{7+\sqrt{5}+\sqrt{2(5+\sqrt{5})}}$	$\frac{2\sqrt{(3+\sqrt{5})(4+\sqrt{2(5+\sqrt{5})})}}{7+\sqrt{5}+\sqrt{2(5+\sqrt{5})}}$
6	21	3	4	28	$\frac{1+2\cos(2\pi/21)}{3+2\cos(2\pi/21)}$	$\frac{4\cos(\pi/21)}{3+2\cos(2\pi/21)}$
6	24	4	2	12	$\frac{\sqrt{2}+\sqrt{6}}{8+\sqrt{2}+\sqrt{6}}$	$\frac{4\sqrt{4+\sqrt{2}+\sqrt{6}}}{8+\sqrt{2}+\sqrt{6}}$
6	26	3	3	26	$\frac{1+2\cos(\pi/13)}{3+2\cos(\pi/13)}$	$\frac{4\cos(\pi/26)}{3+2\cos(\pi/13)}$
6	26	13	1	2	$\frac{\cos(\pi/13)-\cos(2\pi/13)}{2+\cos(\pi/13)+\cos(2\pi/13)}$	$\frac{2\sqrt{(1+\cos(\pi/13))(1+\cos(2\pi/13))}}{2+\cos(\pi/13)+\cos(2\pi/13)}$
6	36	3	2	24	$\frac{1+2\cos(\pi/18)}{3+2\cos(\pi/18)}$	$\frac{4\cos(\pi/36)}{3+2\cos(\pi/18)}$
6	44	4	1	11	$\frac{\cos(\pi/22)}{2+\cos(\pi/22)}$	$\frac{2\sqrt{1+\cos(\pi/22)}}{2+\cos(\pi/22)}$
6	66	3	1	22	$\frac{1+2\cos(\pi/33)}{3+2\cos(\pi/33)}$	$\frac{4\cos(\pi/66)}{3+2\cos(\pi/33)}$

Table 6.1 – continued from previous page

Genus	**m**	**n**	$\mathbf{k_m}$	$\mathbf{k_n}$	$\mathbf{cos}(\alpha_\mathbf{n})$	$\mathbf{sin}(\alpha_\mathbf{n})$
6	24	24	1	1	0	1
6	14	14	2	2	0	1
6	9	9	4	4	0	1
6	8	8	5	5	0	1
6	6	6	10	10	0	1
6	5	5	20	20	0	1
7	5	4	48	60	$\frac{1}{11}(-3+2\sqrt{5})$	$\frac{4\sqrt{3+\sqrt{5}}}{7+\sqrt{5}}$
7	6	4	24	36	$\frac{1}{5}$	$\frac{2\sqrt{6}}{5}$
7	6	5	15	18	$\frac{1}{19}(8-3\sqrt{5})$	$\frac{2\sqrt{6(3+\sqrt{5})}}{9+\sqrt{5}}$
7	7	3	72	168	$\frac{1+2\sin(3\pi/14)}{3+2\sin(3\pi/14)}$	$\frac{2\sqrt{2(1+\sin(3\pi/14))}}{3+2\sin(3\pi/14)}$
7	7	4	16	28	$\frac{\sin(3\pi/14)}{2+\sin(3\pi/14)}$	$\frac{2\sqrt{1+\sin(3\pi/14)}}{2+\sin(3\pi/14)}$
7	8	3	36	96	$\frac{1}{7}(1+2\sqrt{2})$	$\frac{2\sqrt{2+\sqrt{2}}}{3+\sqrt{2}}$
7	8	4	12	24	$\frac{1}{7}(-1+2\sqrt{2})$	$\frac{2\sqrt{10+\sqrt{2}}}{7}$
7	9	3	24	72	$\frac{1+2\cos(2\pi/9)}{3+2\cos(2\pi/9)}$	$\frac{4\cos(\pi/9)}{3+2\cos(2\pi/9)}$
7	9	6	6	9	$\frac{-1+2\cos(2\pi/9)}{5+2\cos(2\pi/9)}$	$\frac{2\sqrt{6(1+\cos(2\pi/9))}}{5+2\cos(2\pi/9)}$
7	10	5	6	12	$\frac{1}{11}(4-\sqrt{5})$	$\frac{2\sqrt{5+2\sqrt{5}}}{4+\sqrt{5}}$
7	10	4	8	20	$\frac{1}{19}(1+2\sqrt{5})$	$\frac{4\sqrt{5+\sqrt{5}}}{9+\sqrt{5}}$
7	10	5	6	12	$\frac{1}{11}(4-\sqrt{5})$	$\frac{2\sqrt{5+2\sqrt{5}}}{4+\sqrt{5}}$

Table 6.1 – continued from previous page

Genus	**m**	**n**	$\mathbf{k_m}$	$\mathbf{k_n}$	$\mathbf{cos}(\alpha_\mathbf{n})$	$\mathbf{sin}(\alpha_\mathbf{n})$
7	12	3	12	48	$\frac{\sqrt{3}}{3}$	$\frac{2\sqrt{2+\sqrt{3}}}{3+\sqrt{3}}$
7	12	4	6	18	$\frac{1}{13}(-3+4\sqrt{3})$	$\frac{2\sqrt{2(2+\sqrt{3})}}{4+\sqrt{3}}$
7	12	6	4	8	$\frac{1}{11}(-4+3\sqrt{3})$	$\frac{2\sqrt{3(2+\sqrt{3})}}{5+\sqrt{3}}$
7	14	3	9	42	$\frac{1+2\cos(\pi/7)}{3+2\cos(\pi/7))}$	$\frac{2\sqrt{2(1+\cos(\pi/7))}}{3+2\cos(\pi/7)}$
7	14	7	3	6	$\frac{\cos(\pi/7)-\sin(3\pi/14)}{2+\cos(\pi/7)+\sin(3\pi/14)}$	$\frac{2\sqrt{(1+\cos(\pi/7))(1+\sin(3\pi/14))}}{2+\cos(\pi/7)+\sin(3\pi/14)}$
7	18	3	6	36	$\frac{1+2\cos(\pi/9)}{3+2\cos(\pi/9)}$	$\frac{2\sqrt{2(1+\cos(\pi/9))}}{3+2\cos(\pi/9)}$
7	15	3	8	40	$\frac{1+2\cos(2\pi/15)}{3+2\cos(2\pi/15)}$	$\frac{4\cos(\pi/15)}{3+2\cos(2\pi/15)}$
7	16	4	4	16	$\frac{\cos(\pi/8)}{2+\cos(\pi/8)}$	$\frac{2\sqrt{1+\cos(\pi/8)}}{2+\cos(\pi/8)}$
7	18	3	6	36	$\frac{1+2\cos(\pi/9)}{3+2\cos(\pi/9)}$	$\frac{2\sqrt{2(1+\cos(\pi/9))}}{3+2\cos(\pi/9)}$
7	18	9	2	4	$\frac{\cos(\pi/9)-\cos(2\pi/9)}{2+\cos(\pi/9)+\cos(2\pi/9)}$	$\frac{\sqrt{5+6\cos(\pi/9)+4\cos(2\pi/9)}}{2+\cos(\pi/9)+\cos(2\pi/9)}$
7	20	4	3	15	$\frac{\sqrt{2(5+\sqrt{5})}}{8+\sqrt{2(5+\sqrt{5})}}$	$\frac{4\sqrt{4+\sqrt{2(5+\sqrt{5})}}}{8+\sqrt{2(5+\sqrt{5})}}$
7	21	6	2	7	$\frac{-1+2\cos(2\pi/21)}{5+2\cos(2\pi/21)}$	$\frac{2\sqrt{6(1+\cos(2\pi/21))}}{5+2\cos(2\pi/21)}$
7	24	3	4	32	$\frac{2+\sqrt{2}+\sqrt{6}}{6+\sqrt{2}+\sqrt{6}}$	$\frac{2\sqrt{2(4+\sqrt{2}+\sqrt{6})}}{6+\sqrt{2}+\sqrt{6}}$
7	28	4	2	14	$\frac{\cos(\pi/14)}{2+\cos(\pi/14)}$	$\frac{2\sqrt{1+\cos(\pi/14)}}{2+\cos(\pi/14)}$
7	30	3	3	30	$\frac{1+2\cos(\pi/15)}{3+2\cos(\pi/15)}$	$\frac{4\cos(\pi/30)}{3+2\cos(\pi/15)}$
7	30	15	1	2	$\frac{\cos(\pi/15)-\cos(2\pi/15)}{2+\cos(\pi/15)+\cos(2\pi/15))}$	$\frac{2\sqrt{(1+\cos(\pi/15))(1+\cos(2\pi/15))}}{2+\cos(\pi/15)+\cos(2\pi/15)}$
7	42	3	2	28	$\frac{(1/2)+\cos(\pi/21)}{(3/2)+\cos(\pi/21)}$	$\frac{4\cos(\pi/42)}{3+2\cos(\pi/21)}$
7	52	4	1	13	$\frac{\cos(\pi/26)}{2+\cos(\pi/26)}$	$\frac{2\sqrt{1+\cos(\pi/26)}}{2+\cos(\pi/26)}$

Table 6.1 – continued from previous page

Genus	**m**	**n**	$\mathbf{k_m}$	$\mathbf{k_n}$	**cos**($\alpha_\mathbf{n}$)	**sin**($\alpha_\mathbf{n}$)
7	78	3	1	26	$\frac{1+2\cos(\pi/39)}{3+2\cos(\pi/39)}$	$\frac{4\cos(\pi/78)}{3+2\cos(\pi/39)}$
7	28	28	1	1	0	1
7	16	16	2	2	0	1
7	12	12	3	3	0	1
7	10	10	4	4	0	1
7	8	8	6	6	0	1
7	7	7	8	8	0	1
7	6	6	12	12	0	1
7	5	5	24	24	0	1

REFERENCES CITED

[1] C. Adams, C. Albors-Riera, B. Haddock, Z. Li, D. Nishida, B. Reinoso, and L. Wang. Hyperbolicity of links in thickened surfaces. *Topology Appl.*, 256:262–278, 2019.

[2] C. Adams, A. Colestock, J. Fowler, W. Gillam, and E. Katerman. Cusp size bounds from singular surfaces in hyperbolic 3-manifolds. *Trans. Amer. Math. Soc.*, 358(2):727–741, 2006.

[3] Colin Adams. Bipyramids and bounds on volumes of hyperbolic links. *Topology Appl.*, 222:100–114, 2017.

[4] Colin Adams, Aaron Calderon, and Nathaniel Mayer. Generalized bipyramids and hyperbolic volumes of alternating k-uniform tiling links. *Topology Appl.*, 271:107045, 28, 2020.

[5] Colin Adams and Eric Schoenfeld. Totally geodesic Seifert surfaces in hyperbolic knot and link complements. I. *Geom. Dedicata*, 116:237–247, 2005.

[6] Colin C. Adams. Toroidally alternating knots and links. *Topology*, 33(2):353–369, 1994.

[7] Ian R. Aitchison and Lawrence D. Reeves. On archimedean link complements. *Journal of Knot Theory and Its Ramifications*, 11(06):833–868, 2002.

[8] Uri Bader, David Fisher, Nicholas Miller, and Matthew Stover. Arithmeticity, superrigidity, and totally geodesic submanifolds. *Ann. of Math. (2)*, 193(3):837–861, 2021.

[9] Andrey Bogdanov, Vadim Meshkov, Alexander Omelchenko, and Mihail Petrov. Classification of textile links, 2007.

[10] Benjamin A. Burton. The next 350 million knots. In *36th International Symposium on Computational Geometry*, volume 164 of *LIPIcs. Leibniz Int. Proc. Inform.*, pages Art. No. 25, 17. Schloss Dagstuhl. Leibniz-Zent. Inform., Wadern, 2020.

[11] Abhijit Champanerkar, Ilya Kofman, and Jessica S. Purcell. Geometry of biperiodic alternating links. *J. Lond. Math. Soc. (2)*, 99(3):807–830, 2019.

[12] Abhijit Champanerkar, Ilya Kofman, and Jessica S. Purcell. Right-angled polyhedra and alternating links. *Algebr. Geom. Topol.*, 22(2):739–784, 2022.

[13] David Coulson, Oliver A. Goodman, Craig D. Hodgson, and Walter D. Neumann. Computing arithmetic invariants of 3-manifolds. *Experiment. Math.*, 9(1):127–152, 2000.

[14] Basudeb Datta and Subhojoy Gupta. Semi-regular tilings of the hyperbolic plane. *Discrete Comput. Geom.*, 65(2):531–553, 2021.

[15] Basudeb Datta and Dipendu Maity. Semi-equivelar maps on the torus and the Klein bottle are Archimedean. *Discrete Math.*, 341(12):3296–3309, 2018.

[16] Allan L. Edmonds, John H. Ewing, and Ravi S. Kulkarni. Regular tessellations of surfaces and $(p,\ q,\ 2)$-triangle groups. *Ann. of Math. (2)*, 116(1):113–132, 1982.

[17] D. B. A. Epstein and R. C. Penner. Euclidean decompositions of noncompact hyperbolic manifolds. *J. Differential Geom.*, 27(1):67–80, 1988.

[18] Benson Farb and Dan Margalit. *A primer on mapping class groups*, volume 49 of *Princeton Mathematical Series*. Princeton University Press, Princeton, NJ, 2012.

[19] David Futer, Emily Hamilton, and Neil R. Hoffman. Infinitely many virtual geometric triangulations. *Journal of Topology*, 15(4):2352–2388, 2022.

[20] Hong-Chuan Gan. Alternating links with totally geodesic checkerboard surfaces. *Algebr. Geom. Topol.*, 21(6):3107–3122, 2021.

[21] Oliver Goodman, Damian Heard, and Craig Hodgson. Commensurators of cusped hyperbolic manifolds. *Experiment. Math.*, 17(3):283–306, 2008.

[22] Branko Grünbaum and Geoffrey C. Shephard. Tilings by regular polygons. Patterns in the plane from Kepler to the present, including recent results and unsolved problems. *Math. Mag.*, 50(5):227–247, 1977.

[23] Sophie L. Ham and Jessica S. Purcell. Geometric triangulations and highly twisted links. *To appear in Algebraic & Geometric Topology*, 2020.

[24] Chuichiro Hayashi. Links with alternating diagrams on closed surfaces of positive genus. *Math. Proc. Cambridge Philos. Soc.*, 117(1):113–128, 1995.

[25] Jim Hoste, Morwen Thistlethwaite, and Jeff Weeks. The first 1,701,936 knots. *Math. Intelligencer*, 20(4):33–48, 1998.

[26] Joshua Howie. *Surface-alternating knots and links*. PhD thesis, University of Melbourne, 2015.

[27] Joshua A. Howie and Jessica S. Purcell. Geometry of alternating links on surfaces. *Trans. Amer. Math. Soc.*, 373(4):2349–2397, 2020.

[28] Efstratia Kalfagianni and Jessica Purcell. Alternating links on surfaces and volume bounds. *To appear in Communications in Analysis and Geometry*, 01 2022.

[29] Marc Lackenby. The volume of hyperbolic alternating link complements. *Proc. London Math. Soc. (3)*, 88(1):204–224, 2004. With an appendix by Ian Agol and Dylan Thurston.

[30] Khanh Le and Rebekah Palmer. Geodesic surfaces in the complement of knots with small crossing number. *arXiv preprint arXiv:2207.14792*, 2022.

[31] Khanh Le and Rebekah Palmer. Totally geodesic surfaces in twist knot complements. *Pacific J. Math.*, 319(1):153–179, 2022.

[32] Alexander Lubotzky and Dan Segal. *Subgroup growth*, volume 212 of *Progress in Mathematics*. Birkhäuser Verlag, Basel, 2003.

[33] Colin Maclachlan and Alan W. Reid. *The arithmetic of hyperbolic 3-manifolds*, volume 219 of *Graduate Texts in Mathematics*. Springer-Verlag, New York, 2003.

[34] G. A. Margulis. *Discrete subgroups of semisimple Lie groups*, volume 17 of *Ergebnisse der Mathematik und ihrer Grenzgebiete (3) [Results in Mathematics and Related Areas (3)]*. Springer-Verlag, Berlin, 1991.

[35] W. Menasco. Closed incompressible surfaces in alternating knot and link complements. *Topology*, 23(1):37–44, 1984.

[36] William Menasco and Alan W. Reid. Totally geodesic surfaces in hyperbolic link complements. In *Topology '90 (Columbus, OH, 1990)*, volume 1 of *Ohio State Univ. Math. Res. Inst. Publ.*, pages 215–226. de Gruyter, Berlin, 1992.

[37] William W. Menasco. Polyhedra representation of link complements. In *Low-dimensional topology (San Francisco, Calif., 1981)*, volume 20 of *Contemp. Math.*, pages 305–325. Amer. Math. Soc., Providence, RI, 1983.

[38] Jeffrey S. Meyer, Christian Millichap, and Rolland Trapp. Arithmeticity and hidden symmetries of fully augmented pretzel link complements. *New York J. Math.*, 26:149–183, 2020.

[39] G. D. Mostow. *Strong rigidity of locally symmetric spaces*. Annals of Mathematics Studies, No. 78. Princeton University Press, Princeton, N.J.; University of Tokyo Press, Tokyo, 1973.

[40] Walter D. Neumann and Alan W. Reid. Arithmetic of hyperbolic manifolds. In *Topology '90 (Columbus, OH, 1990)*, volume 1 of *Ohio State Univ. Math. Res. Inst. Publ.*, pages 273–310. de Gruyter, Berlin, 1992.

[41] Makoto Ozawa. Non-triviality of generalized alternating knots. *J. Knot Theory Ramifications*, 15(3):351–360, 2006.

[42] Carlo Petronio. Ideal triangulations of hyperbolic 3-manifolds. *Boll. Unione Mat. Ital. Sez. B Artic. Ric. Mat. (8)*, 3(3):657–672, 2000.

[43] Gopal Prasad. Strong rigidity of $\mathbb{Q}$-rank 1 lattices. *Invent. Math.*, 21:255–286, 1973.

[44] Jessica S. Purcell. An introduction to fully augmented links. In *Interactions between hyperbolic geometry, quantum topology and number theory*, volume 541 of *Contemp. Math.*, pages 205–220. Amer. Math. Soc., Providence, RI, 2011.

[45] Jessica S. Purcell. *Hyperbolic knot theory*, volume 209 of *Graduate Studies in Mathematics*. American Mathematical Society, Providence, RI, [2020] ©2020.

[46] Alan W. Reid and Genevieve S. Walsh. Commensurability classes of 2-bridge knot complements. *Algebr. Geom. Topol.*, 8(2):1031–1057, 2008.

[47] Jean-Marc Schlenker. Hyperbolic manifolds with polyhedral boundary. *arXiv: Geometric Topology*, 2001.

[48] Kisao Takeuchi. Arithmetic triangle groups. *J. Math. Soc. Japan*, 29(1):91–106, 1977.

[49] William P Thurston. The geometry and topology of three-manifolds. `http://library.msri.org/books/gt3m/`, 1980.

[50] William P. Thurston. Three-dimensional manifolds, Kleinian groups and hyperbolic geometry. *Bull. Amer. Math. Soc. (N.S.)*, 6(3):357–381, 1982.

[51] Akira Ushijima. A volume formula for generalised hyperbolic tetrahedra. In *Non-Euclidean geometries*, volume 581 of *Math. Appl. (N. Y.)*, pages 249–265. Springer, New York, 2006.

[52] Friedhelm Waldhausen. On irreducible 3-manifolds which are sufficiently large. *Annals of Mathematics*, 87(1):56–88, 1968.

[53] Genevieve S. Walsh. Orbifolds and commensurability. In *Interactions between hyperbolic geometry, quantum topology and number theory*, volume 541 of *Contemp. Math.*, pages 221–231. Amer. Math. Soc., Providence, RI, 2011.